MILLIMETER-WAVE INTEGRATED-CIRCUIT ANTENNA ARRAYS

Thesis by

Peter P. Tong

In Partial Fulfillment of the Requirements

for the Degree of

Doctor of Philosophy

California Institute of Technology

Pasadena, California

1985

(Submitted October 12, 1984)

ACKNOWLEDGMENTS

This work could never have been done without the help of many. First I would like to thank God for giving me strength in these four years at Caltech when I needed it. Next I would like to thank my advisor, Dave Rutledge. His constant encouragement ,enthusiasm and excellent guidance in the work stimulated me. Also I would like to thank Dean Neikirk for setting up most of the instruments I used and teaching me how to build integrated-circuits. Moreover, I am indebted to Dr. N. C. Luhmann, Jr. and his group at UCLA especially, Peter Young and Tony Peebles for letting me use their instruments and being very helpful.

For making life more interesting, I would like to thank the guys in the Tai-Yung House (Cheung Kwok Wai, Fai Mok, Ho Chi Fai, Alex Ho and Tang Tin Wu) and the Millimeter-Wave Integrated-Circuit group here at Caltech (Joyce, Chung-en Zah, Wayne Lam, Dayalan Kasilingam, Rick Compton and Wyman Williams). Also my thanks to Mr. and Mrs. B. Lee and their family for helping me to settle down when I first arrived in Los Angeles.

Financially, I would like to thank Caltech for supporting me.

Finally I express my deepest gratitude to my parents, for their unrelentless support.

MILLIMETER-WAVE INTEGRATED-CIRCUIT ANTENNA ARRAYS

ABSTRACT

This thesis presents three different types of millimeter-wave integrated-circuit antenna array. They are a linearly polarized antenna array that can form polarization and intensity line images, a circularly polarized spiral antenna and a two-dimensional tracking antenna array. They are all integrated-circuit antennas with detectors on quartz substrates using quasi-optical systems to collect and focus the waves.

TABLE OF CONTENTS

Table of Contents

Table of Contents

1/INTRODUCTION

Millimeter-wave properties and applications

Millimeter and submillimeter waves have unique properties that make them superior in many applications. They penetrate smoke and dust with less attenuation than the optical and infrared wavelengths. At the same time millimeter and submillimeter wave systems achieve higher resolution with smaller and lighter weight components than their microwave counterparts. One can foresee applications of these wavelengths for short-range communications [1,2] and satellite communications [3,4,5].

Another use of these wavelengths is in fusion experiments in measuring electron density and magnetic fields. Researchers in the fusion experiments are trying to measure the magnetic field in the plasmas by Faraday rotation. These are the natural wavelengths for these measurements because there are problems with refraction at microwave wavelengths and vibration at infrared wavelengths [6,7].

This technology has also been applied productively in the radioastronomy field. It has opened up a new region of the spectrum for interesting observations [8]. These wavelengths are scattered less than shorter wavelengths, and it is also possible to observe

relatively cool objects such as developing stars in large gas clouds.

Existing technologies

Metal waveguides are used at these wavelengths. They become lossy at higher frequencies (about 6 dB/m in rectangular waveguide at 100 GHz). The waveguide dimensions become small and machining becomes difficult and expensive. Also it is hard to mount matching and coupling structures in the small waveguides. In order to get around these problems, we used quasi-optical systems to collect and focus the waves. Integrated-circuit technology is employed to make the antennas and detectors in receivers. This approach gives a flexible design and is relatively inexpensive.

Several millimeter-wave imaging systems have been developed based on a single detector and scanned optics [9,10,11,12]. In many experiments, though, the image may be changing too quickly or there may not be enough integration time for scanned optics. Several workers have proposed imaging arrays [13,14,15], and Neikirk and Rutledge have demonstrated arrays that image intensity at 1.2 mm and 119 μm [16,17].

Overview of the thesis

The polarization of an electric field at millimeter wavelengths is important in many studies and applications including distinguishing man-made and natural objects in radar[18], studying plasmas [6], and suppressing rain echoes [19]. Chapter two of this thesis

will present an intensity and polarization imaging system at a wavelength of 0.8 mm using an array of linearly polarized modified bow-tie antennas. Chapter three presents a millimeter-wave circularly polarized integrated-circuit antenna. In order to form a two-dimensional image with a one-dimensional array, one still needs to scan the array in one direction. However, this scanning can be eliminated as well if a two-dimensional array is available. Chapter four of this thesis will show a two-dimensional tracking antenna array on a dielectric. This array is presently undergoing further development as a GaAs integrated-circuit at the Hughes Aircraft Corporation.

Three separate topics are covered in the Appendices. In Appendix 1, the response of any polarized antenna to any polarized wave is studied. The experimental results fit well with theory. In Appendix 2, the antenna patterns measured at millimeter wavelengths of a long wire antenna on a dielectric are presented together with theory. The final Appendix contains the source code for the program that controls the antenna-pattern measurement.

Part of the work in this thesis has been previously published :

1. P. P. Tong, D. P. Neikirk, D. Psaltis, D. B. Rutledge, K. Wagner and P. E. Young, "Tracking Antenna Arrays for Near-Millimeter Waves." **IEEE Trans. on Antennas and Propagat.**, vol. 31, pp. 512-515, May 1983.

2. P. P. Tong, D. P. Neikirk, P. E. Young, W. A. Peebles, N. C. Luhmann, Jr., and D. B. Rutledge, "Imaging Polarimeter Arrays for Near-Millimeter Waves." **IEEE Trans. on Microwave Theory and Techniques**, vol. 32, pp. 507-512, May 1984.

Bibliography

1. P. G. Steffes and R. A. Meck, "Prototype Tests Secure Millimeter Communications." **Microwave Systems News**, vol. 10, pp. 59-68, October 1980.

2. G. D. O'Clock, Jr., C. Hendrickson, and W. Schaefer, "Optical and MM-Wave Links Face-Off for the Future." **Microwave**, vol. 21, pp. 59-63, March 1982.

3. K. J. Button and J. C. Wiltse (ed.), "Millimeter Systems." Series on **Infrared and Millimeter Waves**, vol. 4, Academic Press, New York, 1981.

4. J. W. Dees, G. P. Kefalas, and J. C. Wiltse, "Millimeter Wave Communications Experiments for Satellite Applications." **Proceedings IEEE International Conference on Communications**, San Francisco, pp. 22-20 to 22-26, June, 1970.

5. "Over $35 Million Sparking 30/20-GHz Satcom." **Microwave Systems News**, vol. 10, pp. 19-22, 26, Oct. 1980.

6. N. C. Luhmann, Jr., "Instrumentation and Techniques for Plasma Diagnostics: An Overview." Series on **Infrared and Millimeter Waves**, vol. 2, Academic Press, New York, 1979.

7. W. Kunz and G. Dodel, "On the Measurement of Poloidal Field Distributions in Tokamaks by Far-infrared Polarimetry." **Plasma Phys.**, vol. 20, pp. 171-174, 1978.

8. J. Eberhart, "Vega and Co.: What's Being Born Out There?" **Science News** 124, pp. 116, 1983.

9. J. P. Hollinger, J. E. Kenney and B. E. Troy Jr., "A Versatile Millimeter-Wave Imaging System." **IEEE Trans. Microwave Theory Tech.** MTT-24, pp. 786-793, 1976.

10. D. T. Hodges, F. B. Foote, E. E. Reber and R. L. Schellenbaum, "Near-millimeter Wave Radiometric imaging." **4th Int. Conf. Infrared Millimeter Waves,** IEEE Cat. No. 79CH1384-7 MTT, p. 49, 1979.

11. J. Waldman, H. R. Fetterman, P. E. Duffy, T. G. Bryant and P. E. Tannenwald, "Submillimeter Model Measurements and Their Applications to Millimeter Radar Systems." **4th Int. Conf. Infrared Millimeter Waves,** IEEE Cat. No. 79CH1384-7 MTT, p. 49, 1979.

12. J. A. Gagliano and J. J. McSheehy, "Airborne Millimeter Wave Radiometer for 94/183 GHz High Altitude Atmospheric Measurements." **6th Int. Conf. Infrared Millimeter Waves,** IEEE Cat. No. 81CH1645-1 MTT, Th-4-6 1981.

13. A. R. Gillespie and T. G. Phillips, "Array Detectors for Millimeter Line Astronomy." **Astron. Astrophys.** 73, p. 14, 1979.

14. K. S. Yngvesson, T. L. Korzeniowski, R. H. Matthews, P. T. Parrish and T. C. L. G. Sollner, "Planar Millimeter Wave Antennas with Application to Monolithic Receivers." **SPIE Proceedings**, vol. 337, Millimeter Wave Technology, 1982.

15. P. T. Parrish, T. C. L. G. Sollner, R. H. Matthews, H. R. Fetterman, C. D. Parker, P. E. Tannenwald

and A. G. Cardiasmenos, "Printed Dipole-Schottky Diode Millimeter Wave Antenna Array." **SPIE Proceedings**, vol. 337, Millimeter Wave Technology, May 1982.

16. D. P. Neikirk, D. B. Rutledge and M. S. Muha, "Far-Infrared Imaging Antenna Arrays." **Appl. Phys. Lett.** 40, pp. 203-205, Feb. 1982.

17. D. P. Neikirk, P. P. Tong, D. B. Rutledge, H. Park and P. E. Young, "Imaging Antenna Array at 119 μm." **Appl. Phys. Lett.** 41, p. 329, 1982.

18. G. R. Valenzuela, "Depolarization of EM Waves by Slightly Rough Surfaces." **IEEE Trans. Antennas Propagat.**, vol. AP-15, pp. 552-557, July 1967.

19. I. M. Hunter, "The Application of a Two Channel Circularly Polarized Radar to the Suppression of Rain Echoes." **Radar Research Establishment Journal**, vol. 36, pp. 1-37, 1955.

2/LINEARLY POLARIZED ANTENNA ARRAY FOR POLARIZATION IMAGING

This chapter presents an integrated-circuit antenna array that images both polarization and intensity. The array consists of a row of antennas that lean alternately left and right, creating two interlaced sub-arrays that respond to different polarizations. The arrays and the bismuth-bolometer detectors are made by a photoresist shadowing technique that requires only one photolithographic mask. The array has measured polarization at a wavelength of 800 μm with an absolute accuracy of 0.8 degrees and a relative precision of 7 arc minutes, and has demonstrated nearly diffraction-limited resolution of a 20-degree step in polarization.

Applications of polarimeters

The polarization of an electric field is important in many studies and applications. Natural objects depolarize a wave while man-made objects do not. The polarization response can separate the two types of radar targets [1]. In plasma studies, both the magnetic field and electron density have to be monitored. The polarization change by Faraday rotation supplies magnetic field information [2]. The same basic idea is used in some semiconductor measurements [3]. In biochemistry, sugar concentration can be measured by the

amount of rotation of the transmitted wave [4].

Some existing polarimeters from optics to microwaves

A variety of different polarimeter schemes have been implemented. In microwaves, two linearly polarized antennas measuring orthogonal components of an electric field form a polarimeter [5]. In optics, the two orthogonal components can be split by a Wollaston prism and measured independently [6]. In millimeter waves, three other methods have been used for plasma diagnostics. In one, the polarization is modulated by a ferrite and one polarization component is measured after it passes through the sample material [7]. Two other schemes avoid the ferrite by frequency mixing techniques. In the first scheme, two waves with slightly different frequencies and opposite circular polarization are combined, generating a wave rotating at the beat frequency [8]. The change in phase due to the wave passing through the sample is proportional to the polarization change. This measurement is independent of fluctuations in source power. In the final scheme, two waves with slightly different frequencies but orthogonal linear polarization are generated [9]. In this last method, the amplitude of the beat signal gives the polarization changes.

In all these methods, imaging can only be done by scanning or by adding more detectors. In this chapter, an integrated circuit antenna array with bolometer detectors will be demonstrated that allows polarization and intensity imaging without scanning at submillimeter wavelengths [10].

The linearly polarized antenna array

Fig. 1 is a drawing of the array designed for a fused-quartz substrate. The antennas slant alternately to the left and right. Fig. 2 is a photograph of an array in its package. All the antennas are linearly polarized. The idea is that there are effectively two interlaced subarrays (left-leaning and right-leaning) that sample two different polarization components of the image. One can recover the two components everywhere by interpolating between samples. Once the two components are known, the polarization can be calculated at all positions.

Antenna spacing for diffraction-limited images

The spacing between antennas should be small enough to achieve the diffraction-limited resolution of the optics. Rutledge et al. show that, in order to achieve diffraction limited resolution in intensity imaging arrays, the intervals must be no greater than $\lambda_d f^{\#}/2$, where λ_d is the dielectric wavelength and $f^{\#}$ is the system f-number [11]. The f-number here is not the conventional f-number f/D, but is defined as $1/2\sin\beta$, where β is half the angle subtended by the exit pupil of the optical system, as seen from the image point. For heterodyne arrays, this spacing doubles. If these sampling criteria are not satisfied, aliasing problems result. In general, for the polarimeter array, the required spacing is halved because each subarray must satisfy the sampling criterion independently. It is a surprising fact, however, that the spacing requirements relax greatly if two conditions are satisfied. If the intensity varies slowly across the object and the

Fig. 1. Polarimeter antenna array designed for use on a fused-quartz substrate ($\varepsilon_r = 4$).

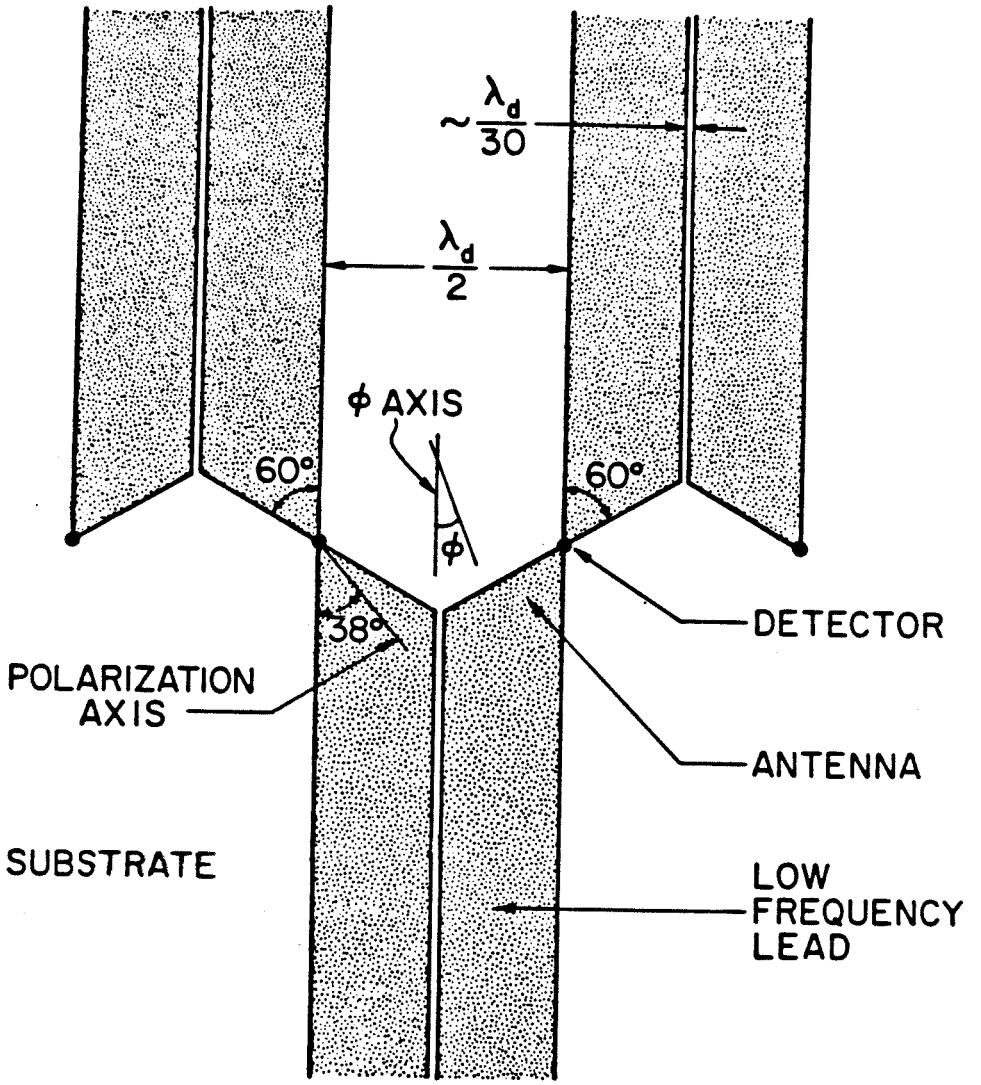

Fig. 2. Linearly polarized antenna array for polarization and intensity measurements in a DIP package.

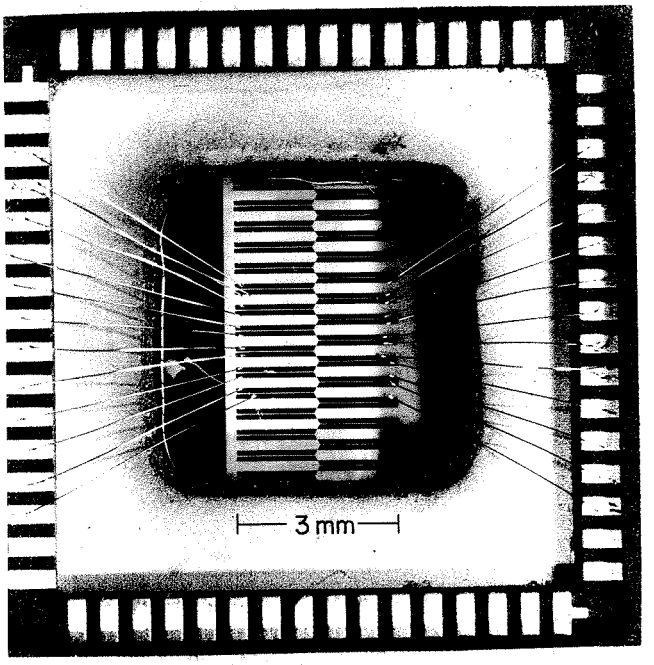

polarization angles are small, then the required spacing is just $\lambda_d f^{\#}$ even for video detection. The reason is that, under these conditions, the changes in the video detector signal become proportional to the electric field and the spacing requirements become those of an ordinary array for heterodyne detection. This is significant in plasma magnetic-field measurements, where the field intensity is kept relatively uniform across the object and the Faraday rotation angles are small (<10 degrees). Later, we will see this effect for a step polarization change of 20 degrees.

To see this mathematically, consider an image which we characterize by an intensity I and polarization angle ϕ that are functions of the position x. The antennas in the polarimeter array receive power P given by

$$P = AI(x)\cos^2(\theta \pm \phi(x)) \qquad (1)$$

where A is the effective area for the antenna and θ is the polarization axis of the antenna. The - sign applies if the antenna leans to the left, and the + sign applies if the antenna leans to the right. For small ϕ, we may write this as

$$P = A(\sin 2\theta)\left(\frac{I}{2\tan\theta} \mp I\phi\right) \qquad (2)$$

If we interpret the power received by each antenna as a sample of the image, and ignore the constant $A\sin 2\theta$, there are two distinct parts of the spatial frequency spectrum of the sampled image, shown in Fig. 3. The spectrum of $I/2\tan\theta$ is centered at f=0 and repeated at multiples of the sampling frequency f_s. The spectrum of $I\phi$, however, is displaced by $f_s/2$. This arises from the alternating + and - sign in (2). The sampling frequency

Fig. 3. The normalized filter response and sampled-image spectra for the array. F_s is the sampling frequency.

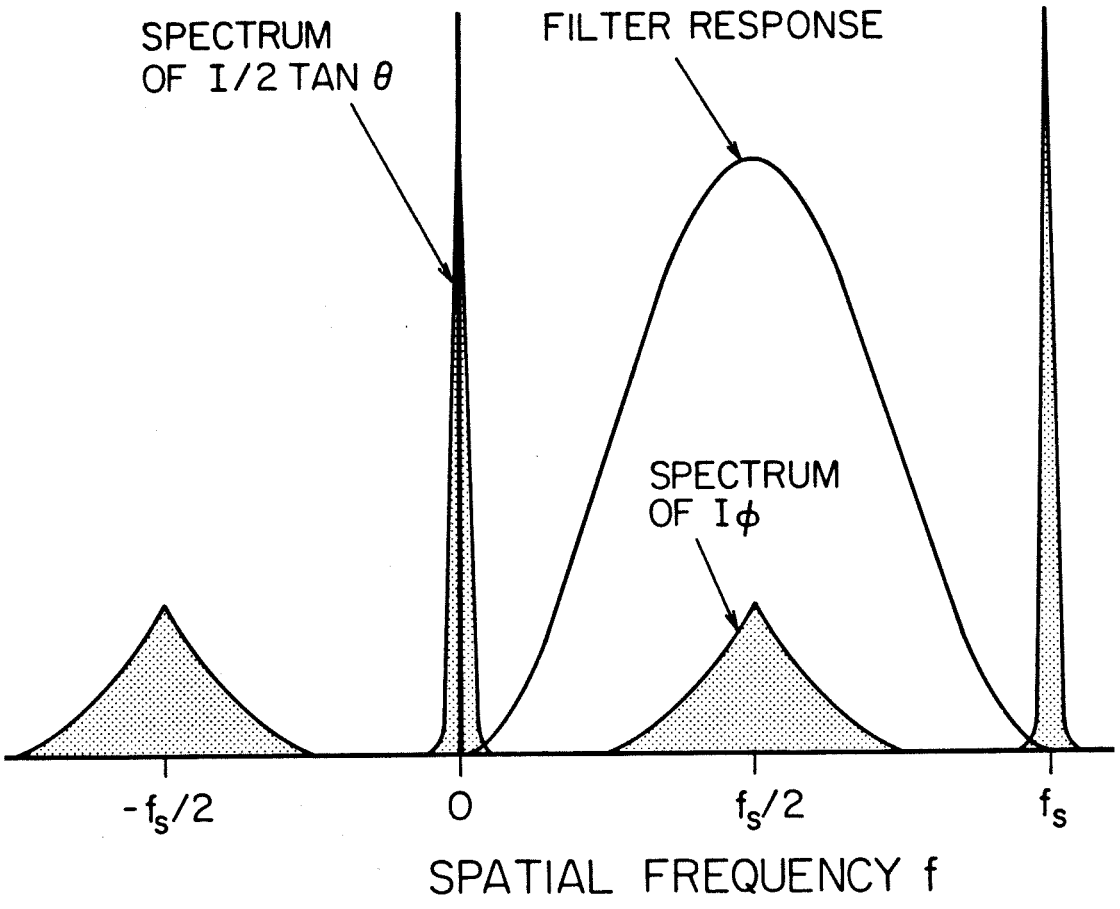

should be large enough so that these spectra do not overlap. This will allow us to recover the polarization angle $\phi(x)$. If I is slowly varying, its spectrum will be narrow band, and the spectrum of $I\phi$ will be only slightly wider than that of ϕ. In this case, f_s must be slightly higher than twice the highest spatial frequency of ϕ. When ϕ is small, it is proportional to the component of the electric field perpendicular to the ϕ-axis as shown in Fig. 1. This means that the diffraction limited cut-off frequency for ϕ is the same as the cutoff frequency for fields given by $1/(2\lambda_d f^{\#})$ [11]. The required sampling period, or antenna spacing, is then $\lambda_d f^{\#}$. This argument has been given for video detection, but the result is the same for heterodyne detection.

To recover ϕ, we filter the data to recover I and $I\phi$ separately, and then divide the latter by I to get the polarization angle ϕ that we seek. In our measurements, where the intensity does not change in time, we normalized the response of each detector so that it was not necessary to filter for I or divide it out. The filter we used to recover ϕ was to take the difference between an antenna signal and the mean of the signals on the adjacent antennas. This gives the normalized filter response $\sin^2(\pi f/f_s)$ shown in Fig. 3.

The design and properties of the antenna array

The array was designed by modeling at the microwave wavelength of 30 mm. The feed patterns for several different planes are shown in Fig. 4. Only the pattern on the dielectric side is shown. The patterns on the air side are at least 10 dB down. The antenna impedance has not been measured, but previous experiments with

Fig. 4. Feed patterns measured on a scale model at 10 GHz.

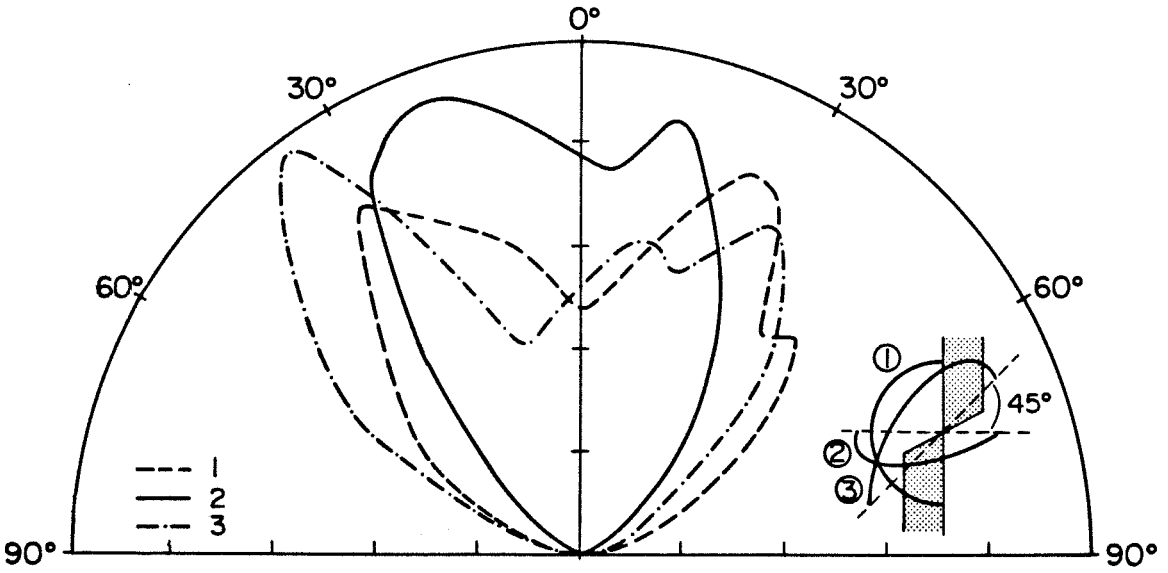

bow-tie antennas indicate that it should be nonresonant with a resistance of 150 Ω. One interesting feature of the array design is the slit between adjacent antennas (see Fig. 1). Without the slit, the antennas were elliptically polarized with an axial ratio (definition at the end of the chapter) of about 3. With the slit, the axial ratio in the microwave measurement was more than 140. After the microwave tests, a scaled-down integrated circuit version was then built for a wavelength of 800 μm.

A photoresist shadowing technique to make the array

The array was fabricated with only one mask and one photoresist exposure by a shadowing technique. The idea was to use a 2 μm wall of photoresist to cast a shadow during the silver evaporation. The photoresist pattern had openings for both the antennas and a 3 μm wide channel connecting the antennas (Fig. 5). Chlorobenzene was used to make an overhanging lip on the photoresist to aid the lift-off process [12]. A silver layer 80 nm thick for the antennas was evaporated first at an angle of 70 degrees. The photoresist wall cast a shadow so that no silver reached the substrate in the channel. Then 200 nm of bismuth were evaporated at normal incidence. The photoresist was removed, leaving behind an antenna array with bismuth bolometers where the channels were previously. One problem arose in fabrication. Often silver strips formed along the wall of the photoresist channel. These did not break when the photoresist was removed and shorted out the bismuth bolometers. This problem was solved by making corners in the photoresist pattern to break the silver strips, so that they were removed with the photoresist (Fig. 6). Fig. 7 shows the finished device. This channel process

Fig. 5. Cross-sectional view showing photoresist channel.

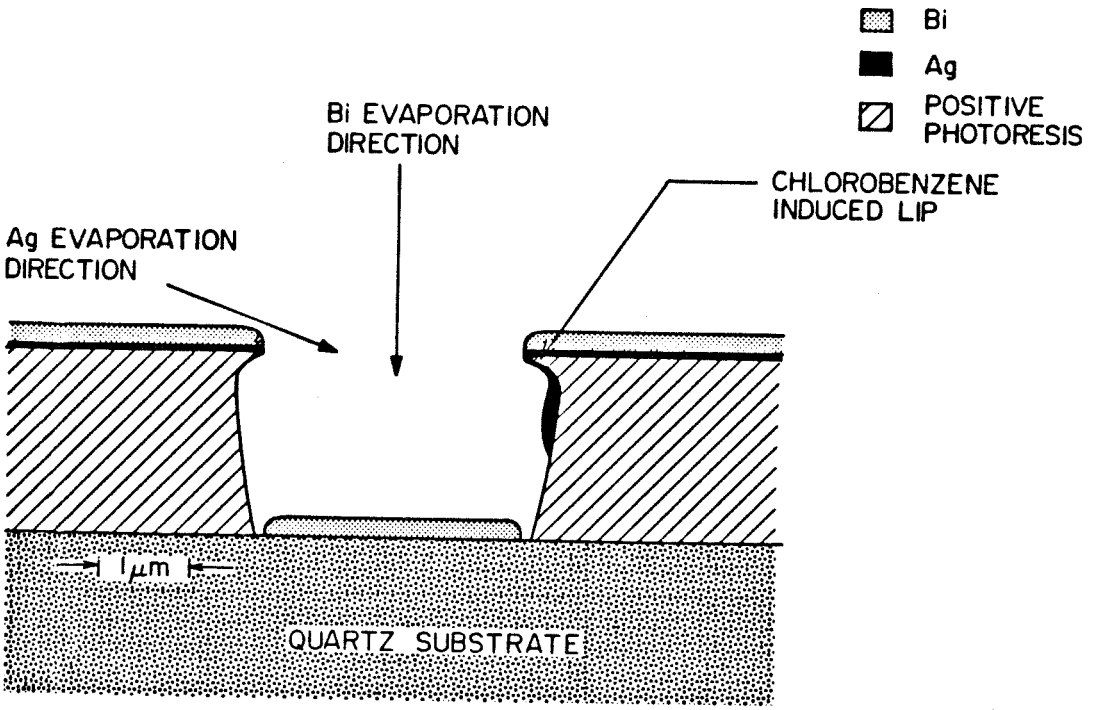

Fig. 6. Top view with photoresist corners that break off silver strips.

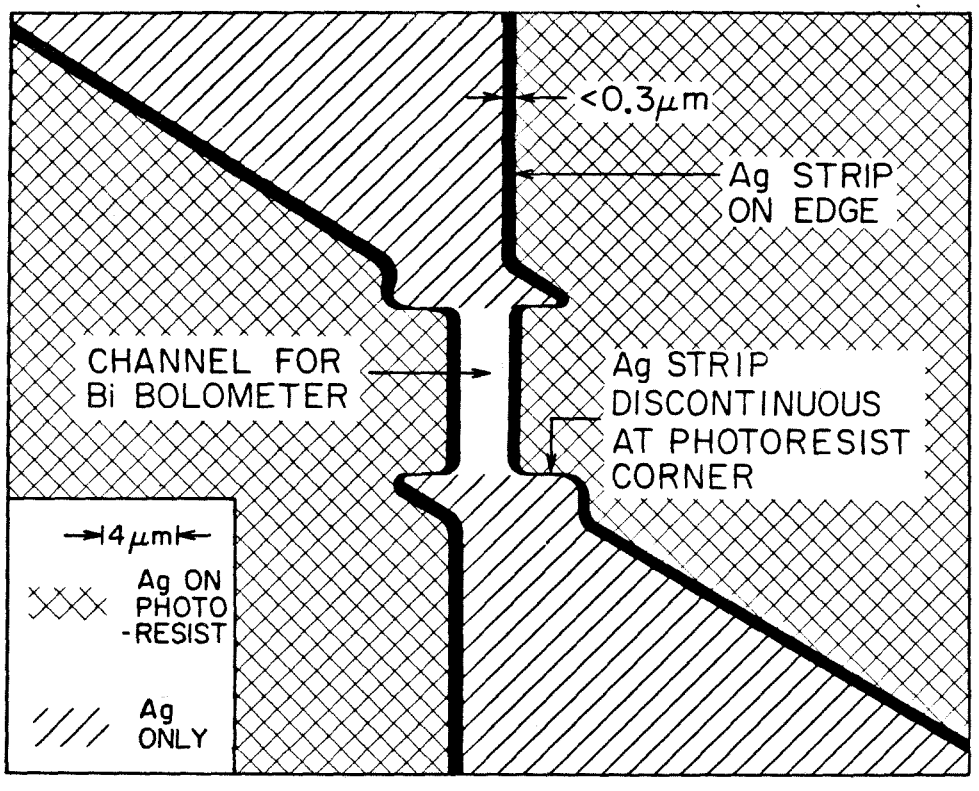

Fig. 7. Photomicrograph with liftoff showing bismuth bolometers. The quartz substrate appears black.

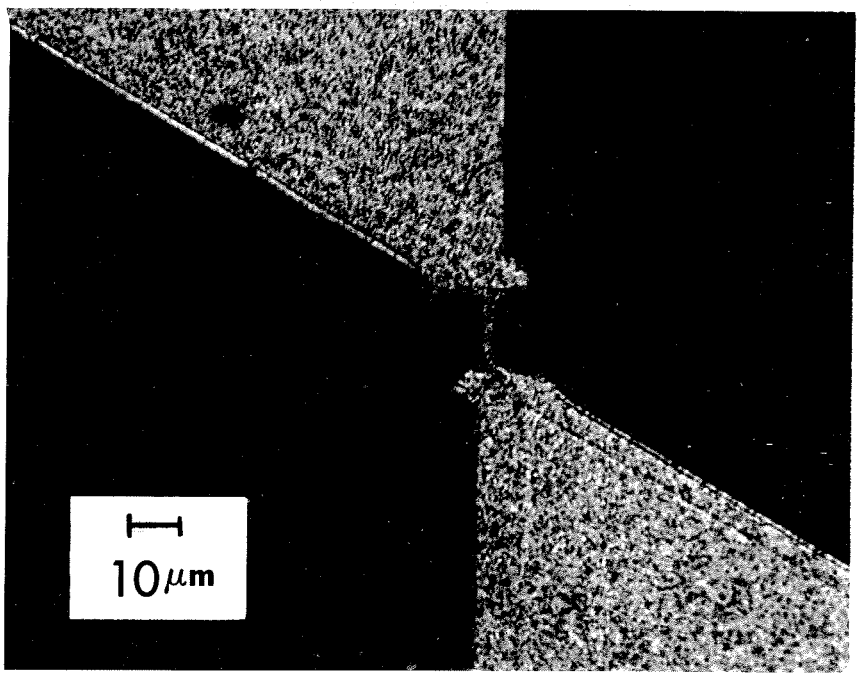

is simpler than the two-step process used to make the two-dimensional tracking antenna array in Chpt. 4. Also the measured electrical NEP is $5 \times 10^{-10} W/(Hz)^{-1/2}$ at a modulation frequency of 100 kHz, which indicates that the detectors have a higher sensitivity as well.

Optical set-up

The polarimeter antenna array was tested at a wavelength of 800 μm in the optical system shown in Fig. 8. The source was a Thomson-CSF carcinotron. A wire-grid polarizer ensured that the beam was linearly polarized [13]. Both the collimator lens and objective lens were made of polyethylene and had a diameter of 11.5 cm and a focal length of 12.7 cm. The beam was chopped at 100 Hz. In two experiments, a crystal-quartz half-wave plate (8.42 mm thick) was used to rotate the polarization a known amount [17]. In the third experiment the half-wave plate was replaced by a chevron aluminum grid as an imaging target. The grid is shown in Fig. 9. The fused-quartz substrate lens had a diameter of 25 mm.

The system $f^{\#}$ was 0.8. For general polarization and intensity imaging, the spacing between the antennas for video detection should be no more than 0.2 λ_d. In our experiments, however, the intensity varied slowly across the array and the polarization angles were small, so that the required spacing is four times larger, 0.8 λ_d. Our array spacing, 0.5 λ_d, satisfied this more relaxed criterion.

The signal captured by the antenna and detector was measured by a model 5204 PAR lock-in. About 5 mW power reached the objective lens. The system responsivity was 0.5 V/W for a 90 Ω bolometer biased at 150 mV.

Fig. 8 Linear polarized antenna array optical set-up.

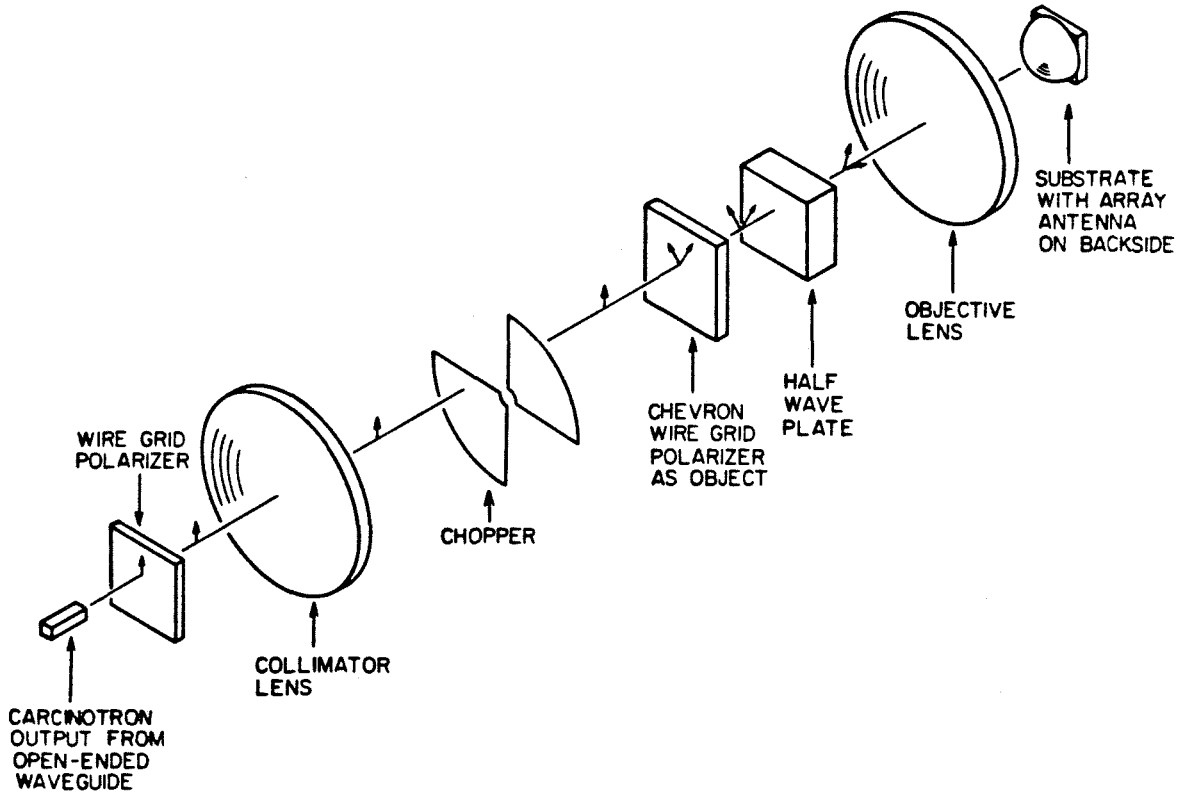

Fig. 9. Photomicrograph of the chevron grid. The light strips are aluminum, 20 μm wide, spaced 20 μm apart, and 300 nm thick. The fused quartz substrate appears black. The grid is made by standard contact photolithography and liftoff.

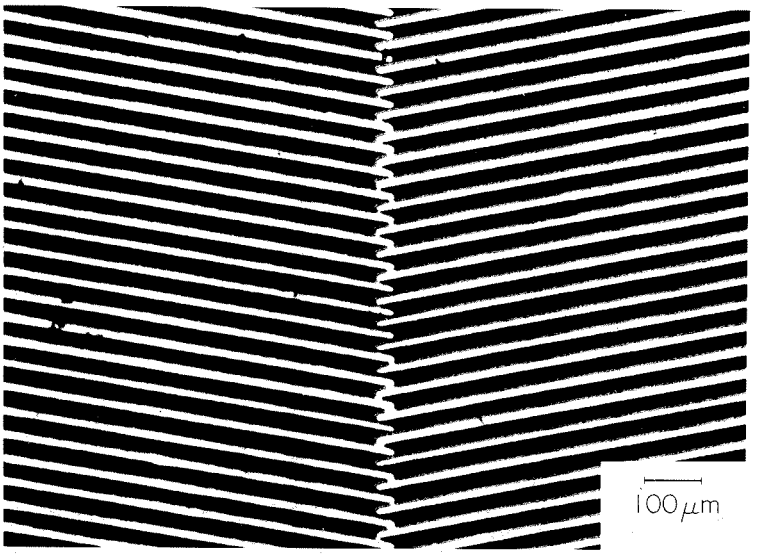

Measuring the polarization angle

Two experiments would be shown here, the first one verified that the antennas were linearly polarized and the second one tested out the response of the array to small angular changes in polarization. From the measurements, the polarization axis was found to be 38 degrees to the left from the ϕ-axis as shown in Fig. 1 for the left-leaning antenna and 38 degrees to the right for the right-leaning antenna. Fig. 10 shows the response of a single antenna to different polarization angles. Comparison with the theoretical cosine-squared curve shows that the antennas are linearly polarized. In the next measurement, the polarization across the object plane was constant, and could be varied by rotating the half-wave plate. Fig. 11(a) shows the measured polarization angle from the array for one setting of the half-wave plate. The standard deviation of the data is 0.8 degree. The change in the measured polarization angle when the half-wave plate was rotated is shown in Fig. 11(b). Here the standard deviation among the data in measuring a 6 degrees change is 5 arc min, and their average value differs from the theoretical value by 7 arc minutes.

Imaging a step change in polarization

The next experiment intended to prove that the array gave diffraction limited images. But before presenting that, this section will first illustrate the theoretical diffraction limited optical response of a step change in polarization. A step change in the polarization of the electric field is generated by a chevron wire grid

Fig. 10. Single antenna response as a function of the polarization angle.

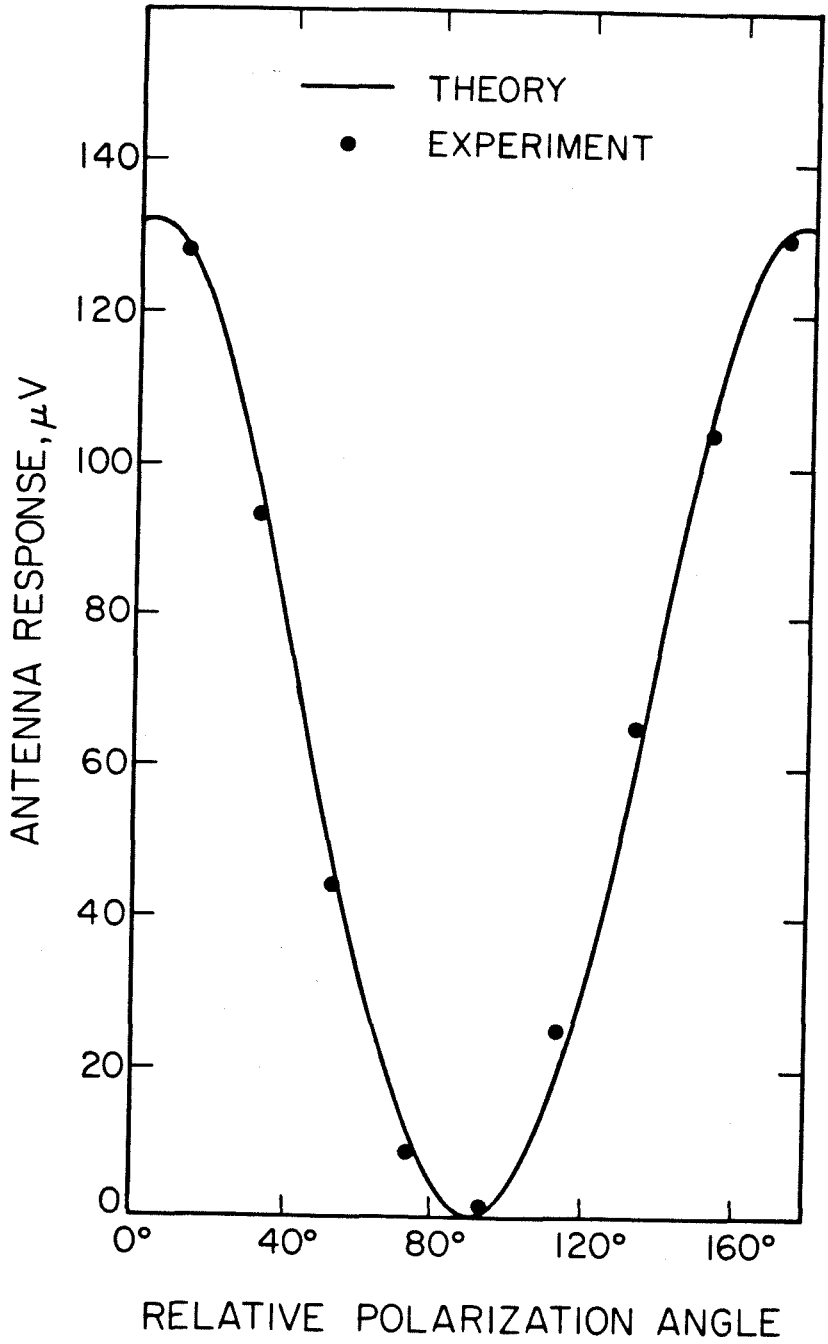

Fig. 11. The array response to small polarization angle. (a) The measured polarization angle for one setting of the half-wave plate. (b) The change in the measured polarization angle caused by rotating the half-wave plate.

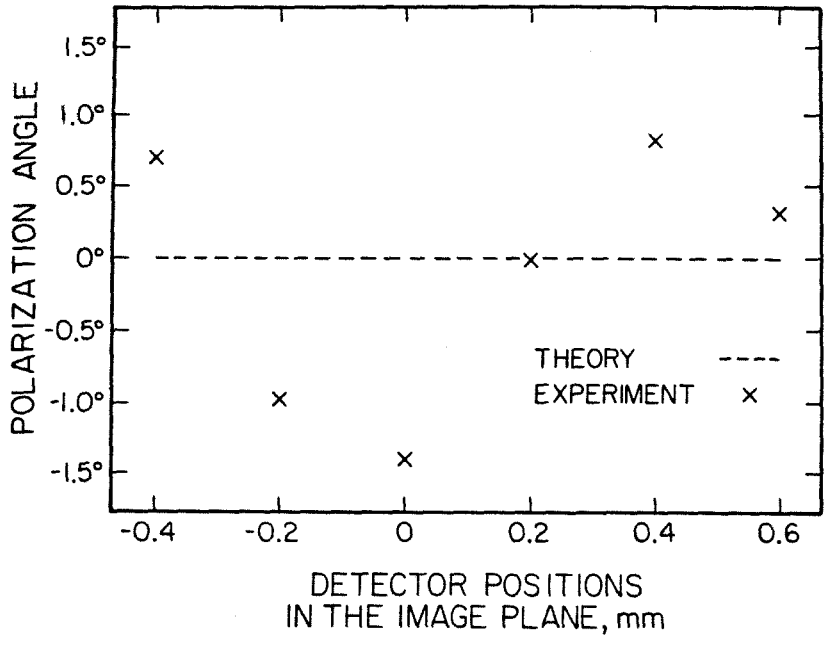

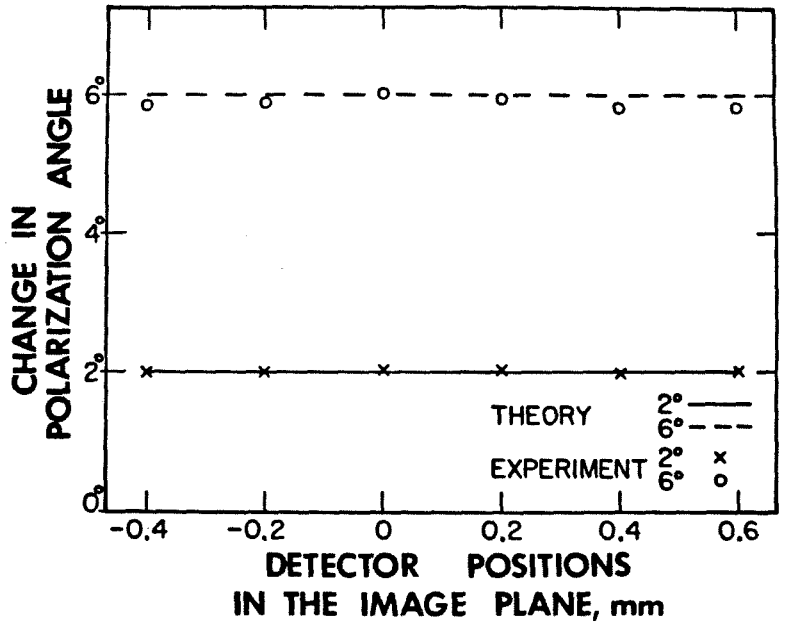

polarizer [13]. Fig. 9 is a photograph of the grid. The frequency of the wave is 375 GHz. The electric field changes from leaning to the left 10 degrees to leaning to the right 10 degrees across the chevron wire grid polarizer.

Fig. 12 shows the co-ordinate system. The electric field just passes through the grid can approximately be resolved into two components:

$$i : \mathrm{sgn}(x) = \begin{cases} 1 & x>0 \\ 0 & \text{for } x=0 \\ -1 & x<0 \end{cases}$$

$$j : 1/(\tan 10^{o}).$$

At the image plane the i^{th} component of the polarization of the electric field can be found by Fourier methods [14] to be:

$$i : \int_{-F}^{F} \left[\int_{-\infty}^{\infty} sgn(x) e^{-j2\pi fx}\, dx \right] e^{j2\pi fx}\, df = \frac{2}{\pi} \int_{0}^{2\pi Fx} \left(\frac{\sin t}{t} \right) dt$$
$$= \frac{2}{\pi} Si(2\pi Fx)$$

with F = electric field cut-off frequency of the optical system.

$= 1/(2\lambda_d f^{\#})$

where λ_d = the dielectric wavelength of the medium in which the image is formed

$f^{\#}$ = system f number. [11]

Si as the Sine integral.

The j^{th} component does not change since it is constant across the whole field of view of the optical system.

Fig. 12. The co-ordinate system for the wire grid.

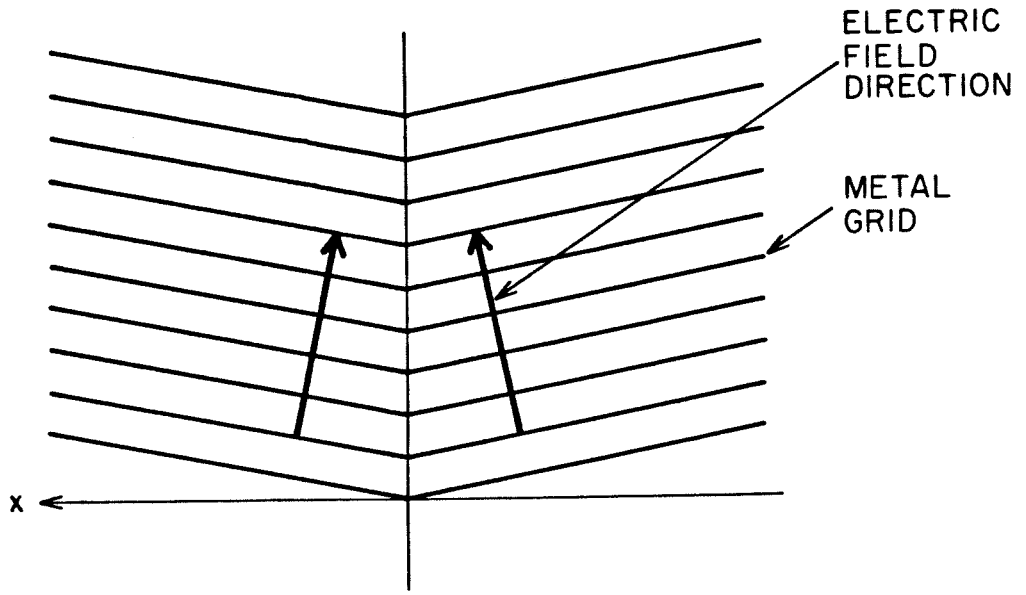

The polarization of the electric field as a function of x can be found by combining the i^{th} and the j^{th} components.

The results are drawn up in Fig. 13 for the optical system given above.

The antenna array imaged the chevron aluminum grid. After the wave passes through the grid, the electric field is perpendicular to the metal lines. This causes a 20 degree step change in polarization at the center of the chevrons. Fig. 13 shows the polarization image, along with the images predicted by geometrical optics (a step change) and by diffraction theory for diffraction limited optics,

$$\phi(x) = \arctan\left[\frac{2}{\pi} Si\left(\frac{\pi x}{\lambda_d f^{\#}}\right) \tan\left(\frac{\phi_o}{2}\right)\right] \qquad (3)$$

where Si is the sine integral [15] and ϕ_o is the step change (20 degrees in this case). The agreement between the experimental points and the diffraction theory indicates that the array is nearly diffraction-limited. This demonstrates that, for slowly varying intensities and small angles, diffraction limited resolution may be achieved by sampling much less often than the general sampling criterion.

Fig. 13. Polarization image of the chevron grid.

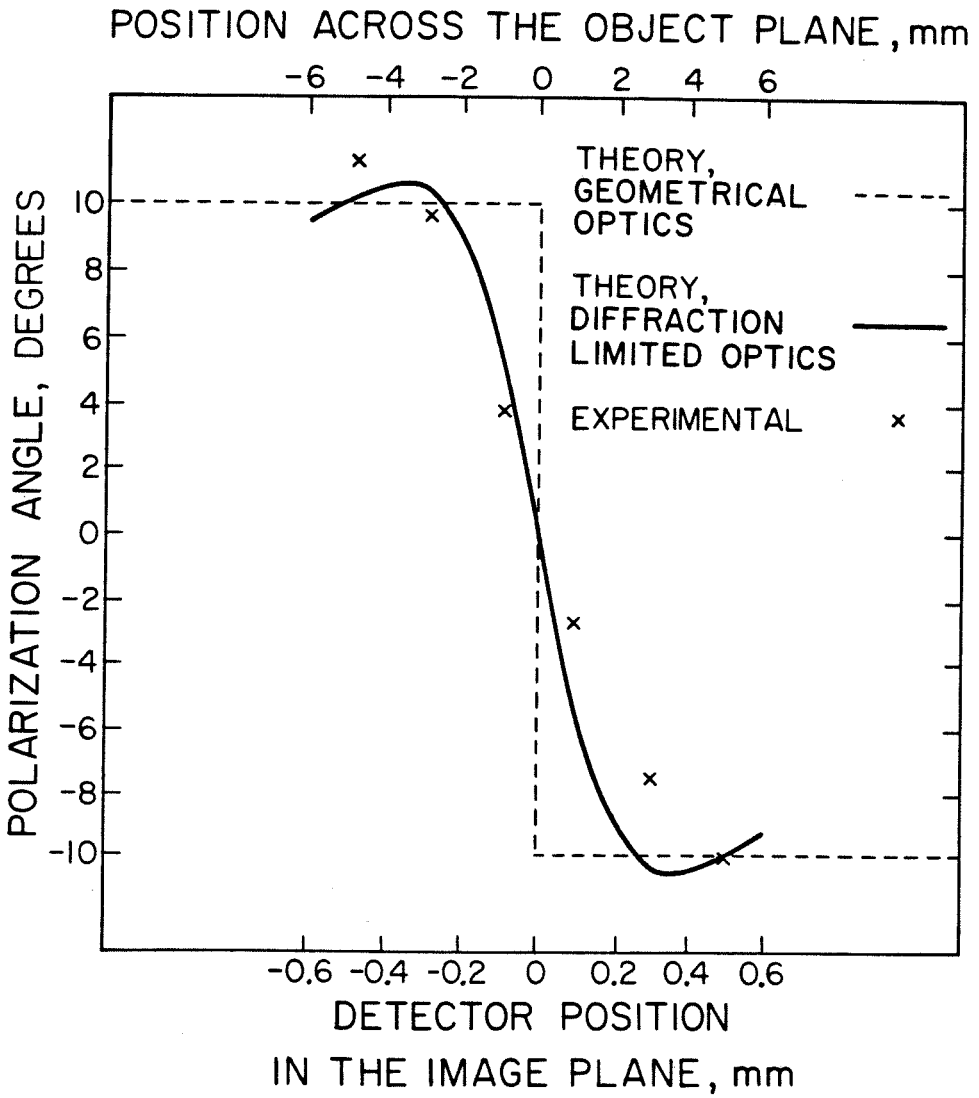

Appendix : common definitions in antenna polarization

Four different terms commonly used will be discussed. They are

1. Axial ratio
2. Ellipticity
3. Eccentricity
4. Cross polarization ratio.

Any polarized electric field can be represented as

$$E = \hat{x} + \delta e^{i\gamma}\hat{y}$$

or as a matrix

$$E = \begin{bmatrix} 1 \\ \delta e^{i\gamma} \end{bmatrix} .$$

The two major axes of an ellipse are related to the above terms by

$$a^2=\cos^2\psi+\delta^2\sin^2\psi+\delta\sin 2\psi\cos\gamma$$

$$b^2=\sin^2\psi+\delta^2\cos^2\psi-\delta\sin 2\psi\cos\gamma$$

where ψ is related to the wave as

$$(1-\delta^2)\sin 2\psi = 2\delta\cos\gamma\cos 2\psi.$$

All these terms are shown in Fig. 14 [16].

Fig. 14. A right-handed circularly polarized (traditional definition) ellipse. The electric field is given by

$$E = \hat{x} - i\hat{y}$$

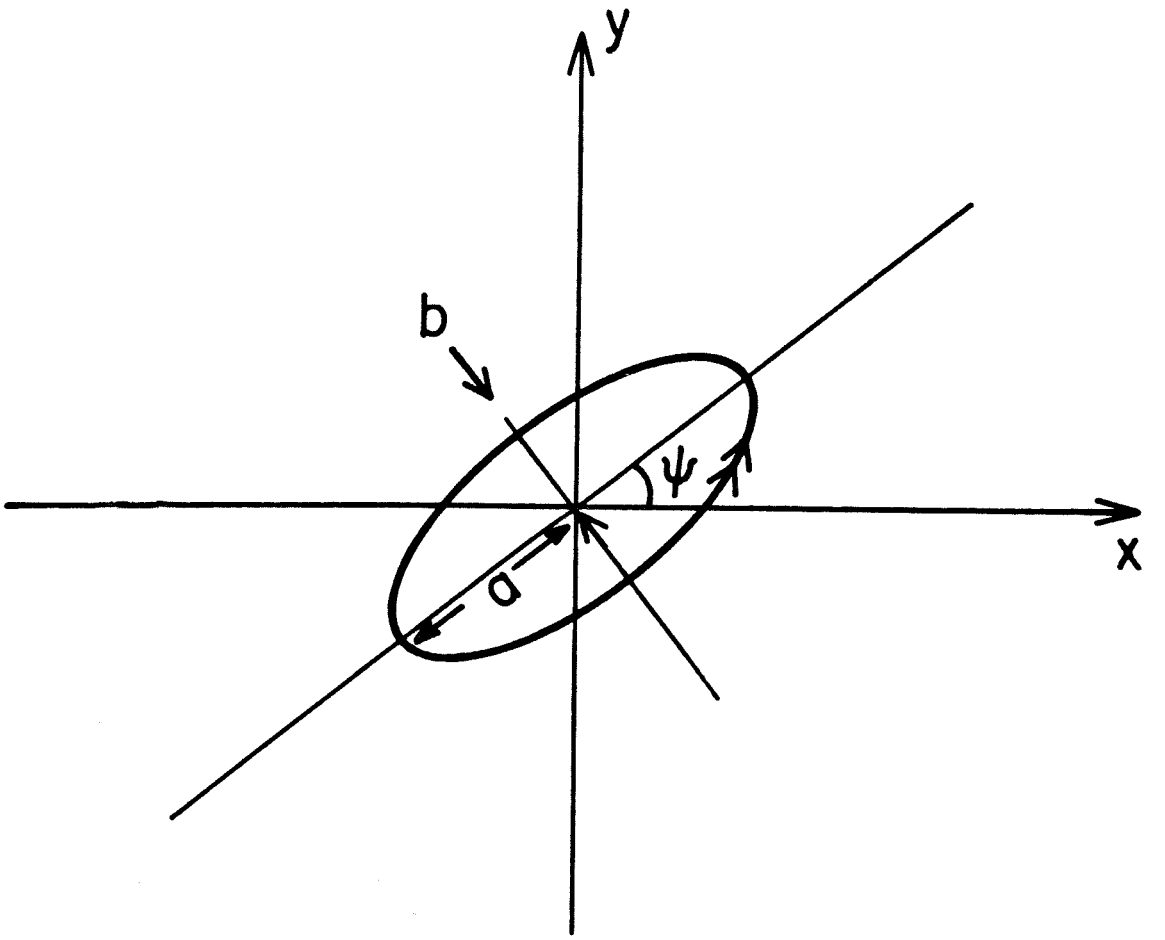

Now the different representations for an elliptical wave or antenna are:

Axial ratio

(Semi-major axis)/(semi-minor axis) = a/b = $1/\mp\tan\Omega$

where $\sin 2\Omega = (\sin 2\alpha)\sin\gamma$

and $\tan\alpha = \delta$.

It may also be defined as

$(E_R+E_L)/(E_R-E_L)$

where E_R = right-hand circularly polarized component of the wave;
E_L = left-hand circularly polarized component of the wave.

Fig. 15 shows the axial ratio of some types of ellipse.

Ellipticity

(Semi-minor axis)/(semi-major axis) = b/a = $\mp\tan\Omega$

Eccentricity

$(1-(b^2/a^2))^{1/2}$

Cross polarization ratio of an antenna

$10\log_{10}$(Max. power received/Min. power received)

One way to get the maximum and minimum power received by

Fig. 15. The axial ratio of a few types of ellipse.

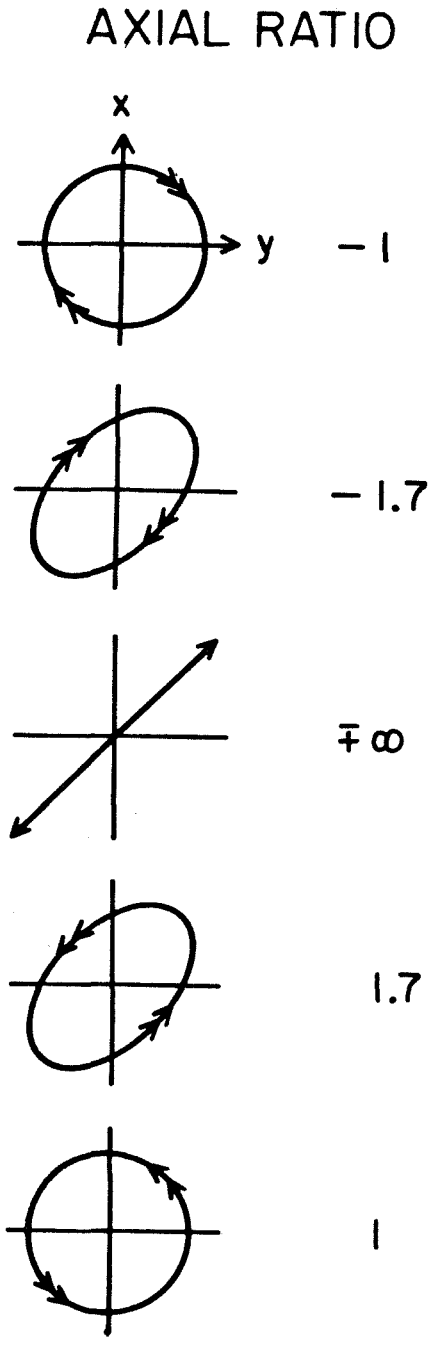

the antenna is by rotating a linearly polarized antenna 180 degrees and monitoring the response of the antenna. The relationship between the axial ratio and the cross polarization ratio is :

$$\text{Cross polarization ratio} = 20\text{Log}_{10}(\text{Axial ratio}).$$

Bibliography

1. G. R. Valenzuela, "Depolarization of EM waves by Slightly Rough Surfaces." **IEEE Trans. Antennas Propagat.**, vol. AP-15, pp. 552-557, July 1967.

2. N. C. Luhmann, Jr., "Instrumentation and Techniques for Plasma Diagnostics: An Overview." Series on **Infrared and Millimeter waves**, vol. 2, Academic Press, New York, 1979.

3. E. K. Galanov, G. N. Potikhonov, V. V. Sorokhin, and O. M. Sheshin, "Infrared Polarimeters and Questions of Method Relating to Contactless Measurement of Free-carrier Concentrations in Semiconductors." **Ind. Lab.**, vol. 42, pp. 1530-1533, Oct. 1976.

4. J. W. Gates, "An Automatic Recording Saccharimeter." **Chem. Ind.**, pp. 190-193, Feb. 1958.

5. S. Suzuki and A. Tsuchiya, "A Time-sharing Polarimeter at 200 MC." **IRE Proc.**, vol. 46, pp. 190-194, Jan. 1958.

6. E. Hecht and A. Zajac, **Optics**, 4th edition. Addison-Wesley. Feb. 1979, p. 238.

7. C. H. Ma, D. P. Hutchinson and K. L. Vander Sluis "A Modulated Submillimeter-laser Polarimeter for the Measurement of the Faraday Rotation by a Plasma." **Appl. Phys. Lett.**, 34, pp. 218-220, Feb. 1979.

8. G. Dodel and W. Kunz, "A Far-infrared 'Polari-interferometer' for Simultaneous Electron Density and Magnetic Field Measurements in Plasmas." **Infr. Phys.**, vol. 18, pp. 773-776, 1978.

9. H. Soltwisch and T. F. R. Equipe, "Experimental Test of Far-infrared Polarimetry for Faraday Rotation Measurements on the TFR 600 Tokamak." **Infr. Phys.** vol. 21, pp. 287-298, 1981.

10. P. P. Tong, D. P. Neikirk, P. E. Young, W. A. Peebles, N. C. Luhmann, Jr. and D. B. Rutledge, "Imaging Polarimeter Arrays for Near-Millimeter Waves." **IEEE Trans. on Microwave Theory and Tech.**, vol 32, pp. 507-512, May 1984.

11. D. B. Rutledge, D. P. Neikirk, and D. P. Kasilingam, "Integrated Circuit Antennas." Series on **Infrared and Millimeter Waves**, vol. 10, Academic Press, New York.

12. M. Hatzakis, B. J. Canavello, and J. M. Shaw, "Single-step Optical Lift-off Process." **IBM J. Res. Develop.**, vol. 24, pp. 452-460, July 1980.

13. G. R. Bird and M. Parrish, Jr., "The Wire Grid as a Near-infrared Polarizer." **J. Opt. Soc. Am.**, vol. 50, pp. 886-891, Sept. 1960.

14. J. W. Goodman, **Introduction to Fourier Optics.** New York: McGraw-Hill, Chpt. 6, 1968.

15. M. Abramowitz and I. A. Stegun, **Handbook of Mathematical Functions.** Dover Publication, New York, Chpt. 5, 1965.

16. M. Born and E. Wolf, **Principles of Optics**, 6th edition. Pergamon Press, Chpt. 1.

17. F. A. Jenkins and H. E. White, **Fundamentals of Optics**, 4th edition. New York, McGraw-Hill, 1976, p. 567.

3/CIRCULARLY POLARIZED SPIRAL ANTENNA ARRAY

This chapter discusses the performance of a circularly polarized antenna on a dielectric. It is an equiangular spiral antenna. The axial ratio, antenna patterns and efficiency of the antenna will be presented. Also a new antenna pattern measurement technique in the millimeter waves for integrated-circuit antennas will be shown.

Circularly polarized spiral antenna : motivation

Circularly polarized antennas are attractive for many applications. Because of their spherical shape, their reflections reverse the sense of an incident circular polarized wave, and so a circular-polarized radar can suppress much rain clutter [1]. Also they give identical response to a linearly polarized wave whose electric field is at any orientation.

Fig.1 shows the circularly polarized spiral antenna on quartz. Its E and H plane antenna patterns have 3 dB beamwidths less than 12 degrees. Measurements indicate that the efficiency is quite high, 86%. This is much better than the performance previously reported for bow-tie, which is around 25%.

Fig.1 Circularly polarized antenna array in a DIP package.

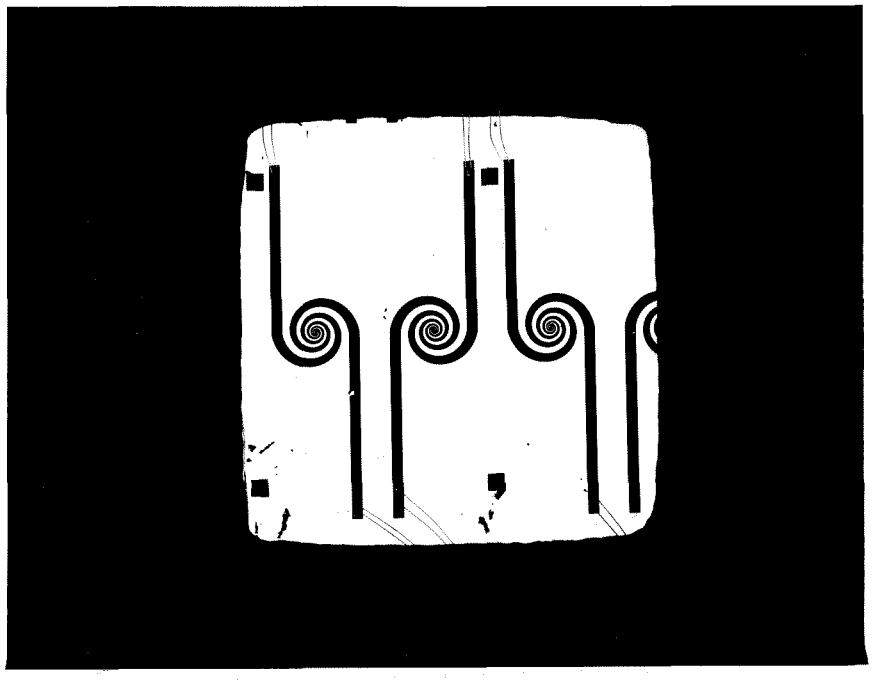

The equiangular spiral antenna in free space

The equiangular spiral antenna in free space has previously been studied [2]. The antenna can be described in polar co-ordinates by the equation,

$$r = ke^{a(\phi-\alpha)}. \qquad (1)$$

It is called equiangular because the angle between the slope of the curve and the radius is always a constant. It is given by,

$$\cos\theta = a/(a^2+1)^{1/2}$$

where θ is as shown in Fig. 2.

It is a frequency-independent antenna since all shapes are described in terms of angles [3]. Bandwidth in excess of 20 to 1 has been achieved.

The design and impedance of the spiral on dielectric

The integrated-circuit spiral antenna on quartz has the same shape as the free space spiral. A lens was placed on the back of the substrate. This substrate lens takes advantage of the fact that antennas are most sensitive to radiation from the substrate side [4]. Fig. 3 shows the design of the antenna on a substrate with a dielectric constant of 4. It has been found experimentally that the antenna will be circularly polarized (axial ratio < 1.2) if the detector length is less than 0.04 λ_d and the antenna is more than 1.25 λ_d in diameter. λ_d is the dielectric wavelength. Fig. 3 shows a photograph of a few of the antennas in an integrated-circuitpackage.

Fig. 2. An equiangular spiral.

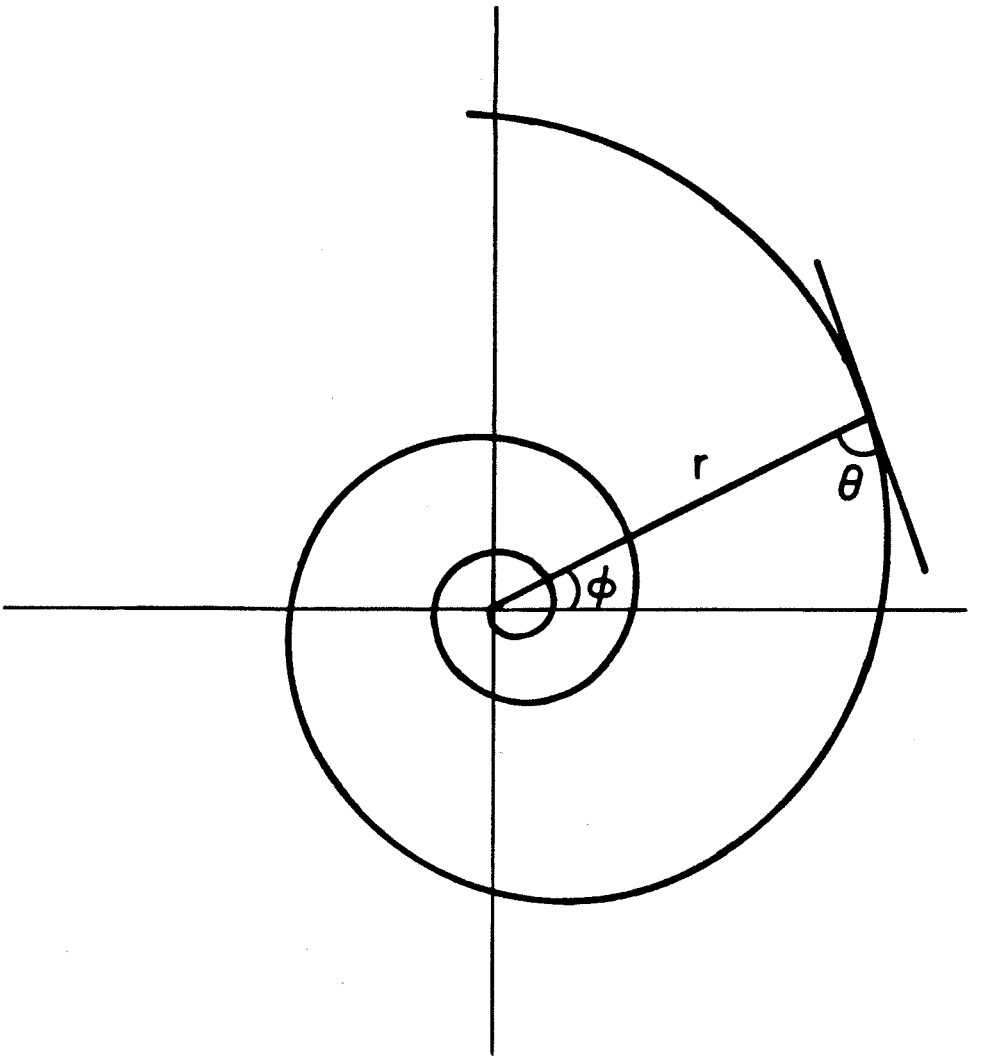

$$r = ke^{a(\phi - \alpha)}$$

Fig. 3. Circularly polarized equiangular spiral antenna designed for use on a fused-quartz substrate ($\varepsilon_r = 4$).

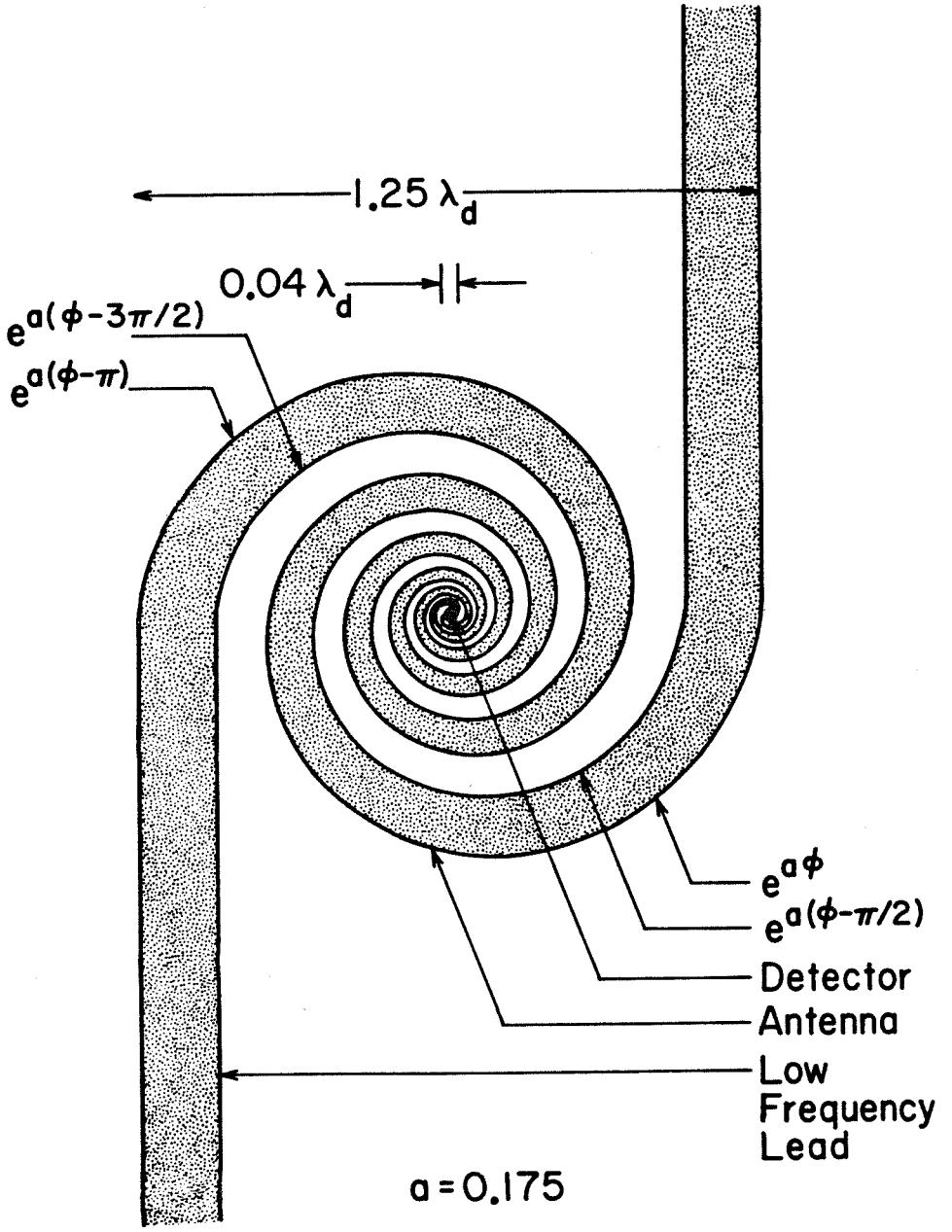

The distance between the antennas is 0.42 λ_d. The antenna is self-complementary [5]. We can estimate its impedance as [6],

$$Z^2 = \eta^2/4$$

where $\eta = \eta_o/(\varepsilon)^{1/2}$

with η_o = the impedance of the free space,

and ε = mean of the two dielectric constants.

With fused quartz as the substrate, the terminal impedance is close to 120 Ω. Bi bolometers serve as the detectors. The leads extending from the edge of the spiral are for biasing and low-frequency detection.

Integrated-circuit fabrication of the spiral

The spiral antenna is made by integrated-circuit techniques. An HP plotter drew the mask for the spiral. The integrated-circuit was then made by lift-off techniques. The antennas are made of silver two thousand angstroms thick. A chlorobenzene process [7] improved the lift-off edges. Two thousand angstroms of Bismuth were then evaporated at a 45-degree angle to help solve the step coverage problem [8]. Fig. 4 is a photomicrograph of the antenna with a Bi bolometer at the middle. The resistance of the bolometer is about 170 Ω.

Three characteristics of the antenna -- antenna axial ratio, antenna pattern and the efficiency of the spiral will be presented.

Fig. 4. Photomicrograph of one spiral antenna. The bright area is the silver antenna while the dark area is the quartz substrate. The dark line in the middle is a Bi bolometer.

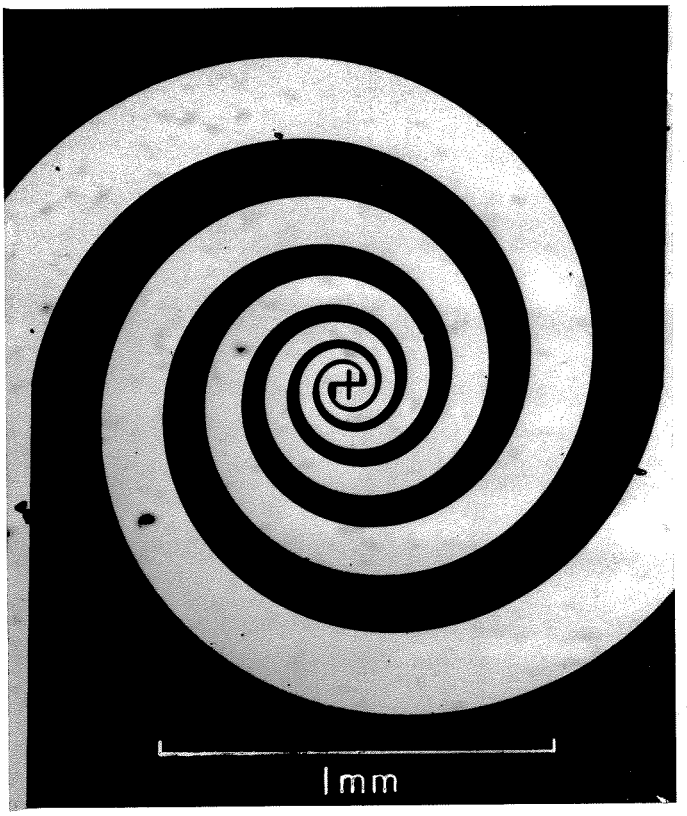

The axial ratio of the spiral on dielectric.

Axial ratio of an ellipse is defined as

(Semi-major axis)/(semi-minor axis).

It may also be defined as

$(E_R+E_L)/(E_R-E_L)$

where E_R = right-hand circularly polarized component of the wave.
E_L = left-hand circularly polarized component of the wave.

Fig. 5 shows the optical set-up to measure the antenna axial ratio in 94 GHz. The source was a linearly polarized radiation at 94 GHz. The wave was electronically modulated at 1 kHz. It was collimated and passed through a quarter-wave plate and an objective lens and received by the spiral antenna at the back of a substrate lens. The objective lens is made of polyethylene with a 15-inch focal length and a 6-inch diameter. The substrate lens is aplanatic [9], and is made of fused quartz with a 1.97-inch radius. The quarter-wave plate is of crystal quartz [10]. Depending on its orientation, it changes a linearly polarized wave from linear to elliptical to circular wave. The theoretical response of a circularly polarized antenna to the above set-up is

$$P_r \propto 1-\sin 2\theta$$

where θ is the angle between the optical axis and the direction perpendicular to the linearly polarized wave as shown in Fig. 6 and

Fig. 5. The optical set-up to test the response of the antenna to an elliptically polarized wave.

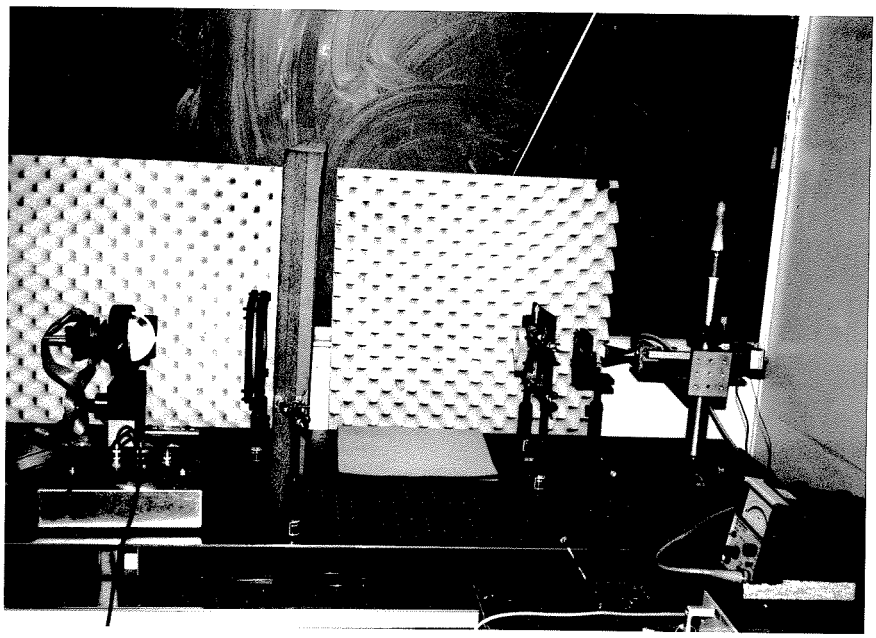

Fig. 6.The relationship between the incident electric field direction and the orientation of the uniaxial crystal.

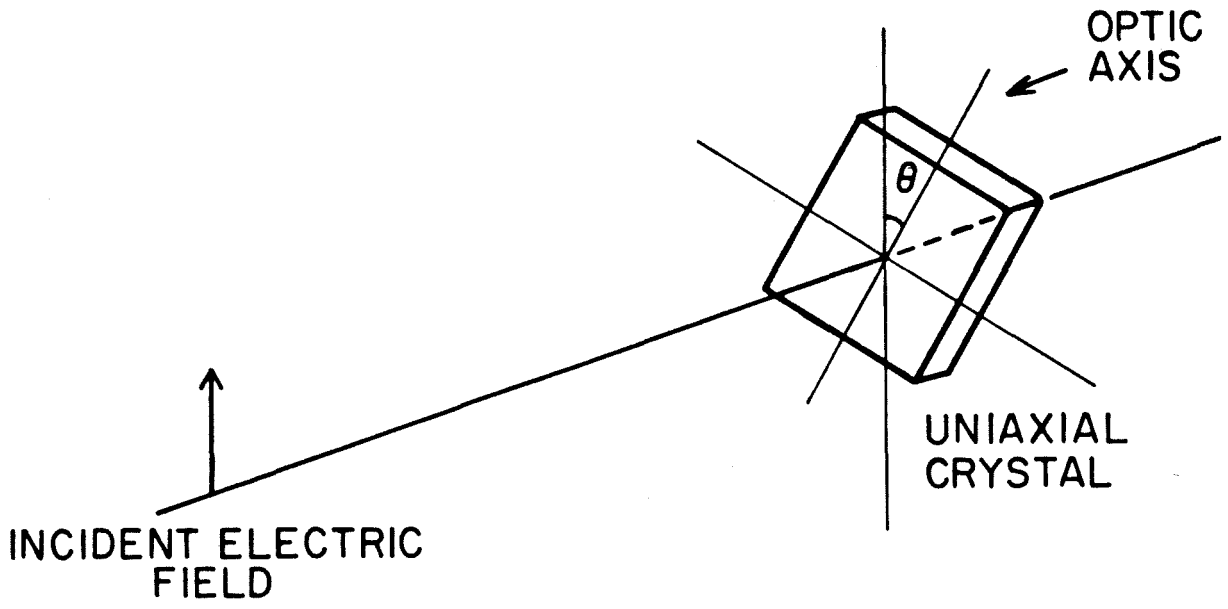

P_r = power received by the antenna.

Fig. 7 shows the theoretical and experimental results. The axial ratio of the antenna is less than 1.2.

Antenna pattern measurements at millimeter wavelengths

A quasi-optical system is used to measure the antenna pattern of an integrated-circuit antenna on a dielectric. The dielectric antenna is positioned at the center of the radius of curvature of a hemisphere, so that any rays reaching the antenna are not refracted by the hemispherical lens. By rotating the lens about its center of the radius of curvature, one can measure the antenna response to different directions. This will then give the antenna pattern. Fig. 8 shows the idea.

There are a few things that one has to pay attention to in pattern measurements. First, the set-up has to be in an anechoic chamber as shown in Fig. 9. Absorbers (supplied by Plessey) are needed at the back of the hemisphere as well. The antenna should be carefully centered.

Fig. 10 is a diagram of the optical set-up together with the data-collecting instruments to measure the patterns of the antennas in the millimeter wavelengths. A klystron transmitted a 94 GHz wave through a 24 dB gain horn. The horn had a 1 inch by 1 inch mouth. The wave was electronically modulated at 1 kHz. A hemispherical lens was placed 30 inches away from the mouth of the horn. The lens was made of fused quartz with a 1.97 inch radius. Fig. 11(a) is a picture of the lens in its holder with two stepper motors, one on the side and the other at the bottom. The motor can give 4 steps per

Fig. 7. The theoretical and experimental response of the antenna to elliptically polarized wave.

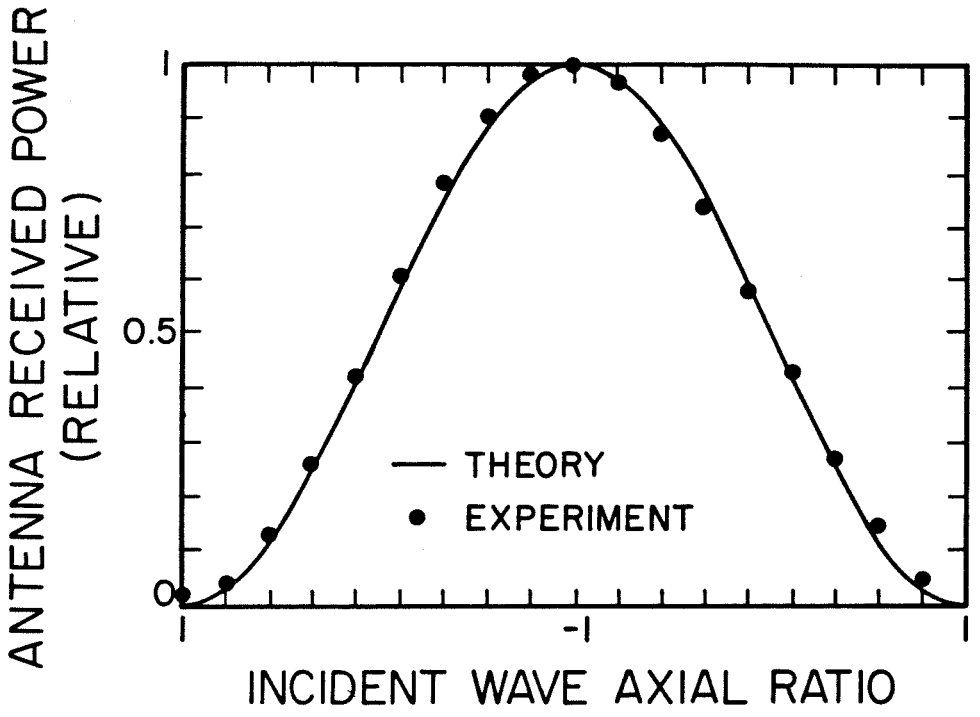

Fig. 8. Antenna pattern measurement idea.

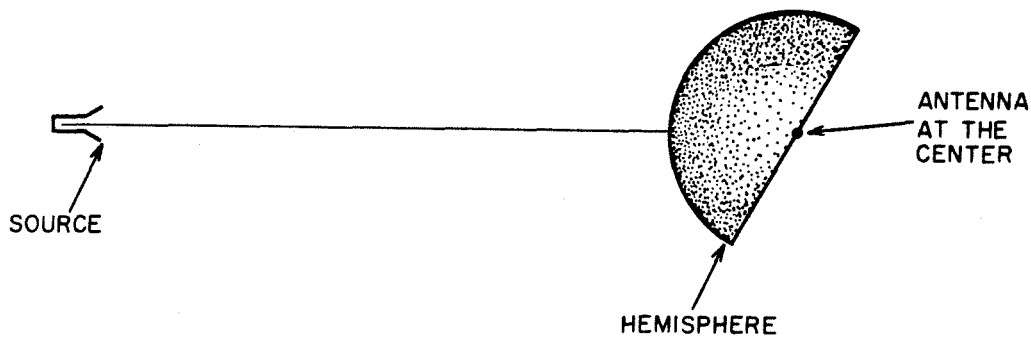

Fig. 9. Photograph of the antenna pattern measurement optical set-up in an anechoic chamber.

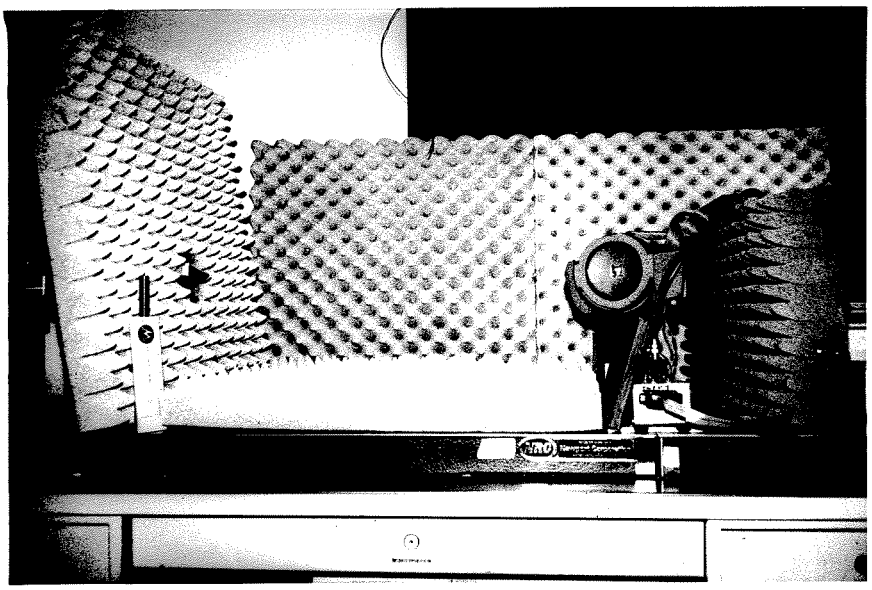

Fig. 10. Diagram of the optical set-up together with the data-collecting instruments.

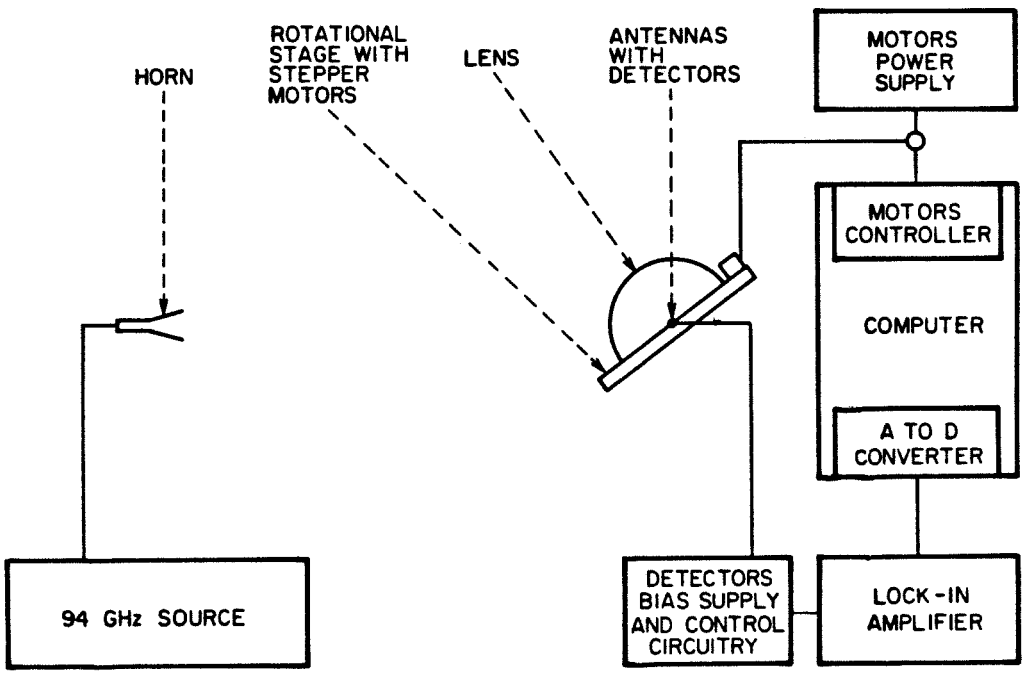

degree. Each motor needs a 28 V and 2 A power supply. The lens could be rotated by the stepper motors about its center of curvature in both the θ and ϕ directions in the spherical co-ordinates. The stepper motors were controlled by an IBM personal computer through a Tecmar PC-Mate Stepper Motor Controller. Fig. 11(b) shows the lens with the antennas. As the lens rotated, the antenna would couple in different power corresponding to its pattern. The power was amplified by a Princeton Applied Research Model 124A Lock-In Amplifier with a model 118 Differential Preamplifier. Then the signal was fed to the same personal computer through a Data Translation Model 2801 analog to digital converter. Data were stored and manipulated as desired. The program to rotate the stepper motors and then take the data is as shown in Appendix 3.

The measurement methods and set-up were tested out by measuring the antenna patterns of a long wire antenna on a dielectric. It was described in Appendix 2. The results give us confidence in the measured patterns.

The antenna patterns of the spiral on dielectric

Fig. 12 gives the two principal patterns of the spiral antenna. Due to symmetry of the spiral, the two patterns should be identical. Both of them had a center peak. The E-plane 3 dB beamwidth was 11.5 degrees, while the H-plane 3 dB beamwidth was 8.5 degrees. In comparison, the narrowest 3 dB beamwidth of the modified bow tie array in Chapter 2 was 67 degrees and the two-dimensional array in Chapter 4 was 34 degrees.

Fig. 11(a). Hemispherical lens in its holder showing the two stepper motors.

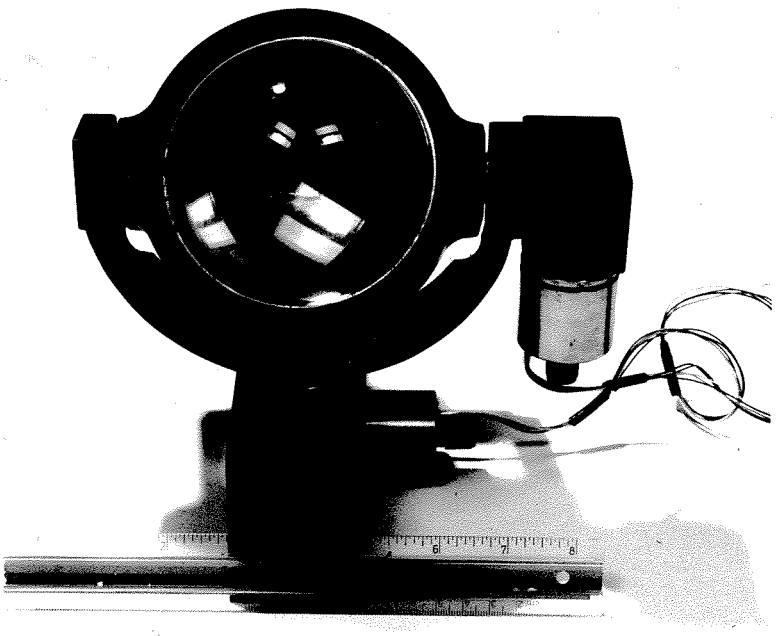

Fig. 11(b). Lens with the antennas.

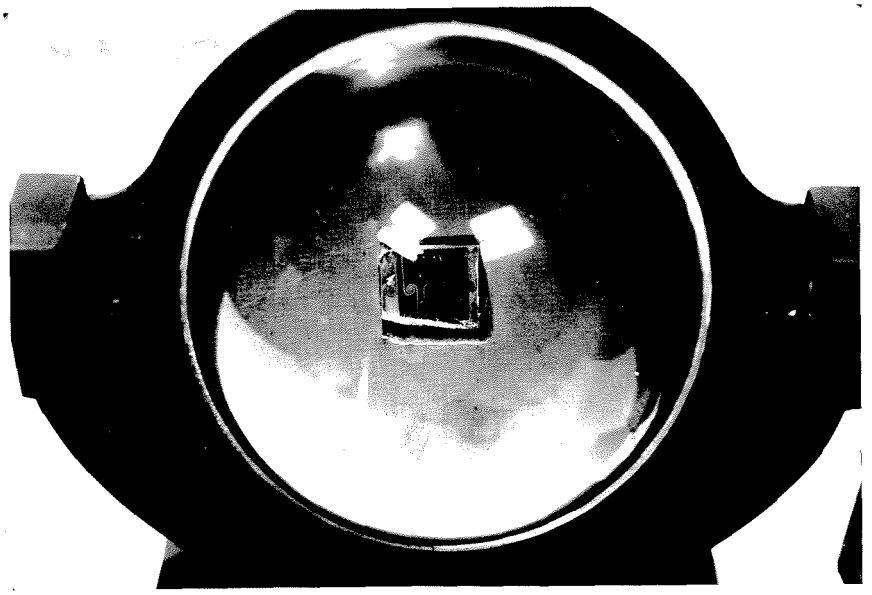

Fig. 12. The antenna patterns of the spiral antenna. Experimental points were taken every 2 degrees.

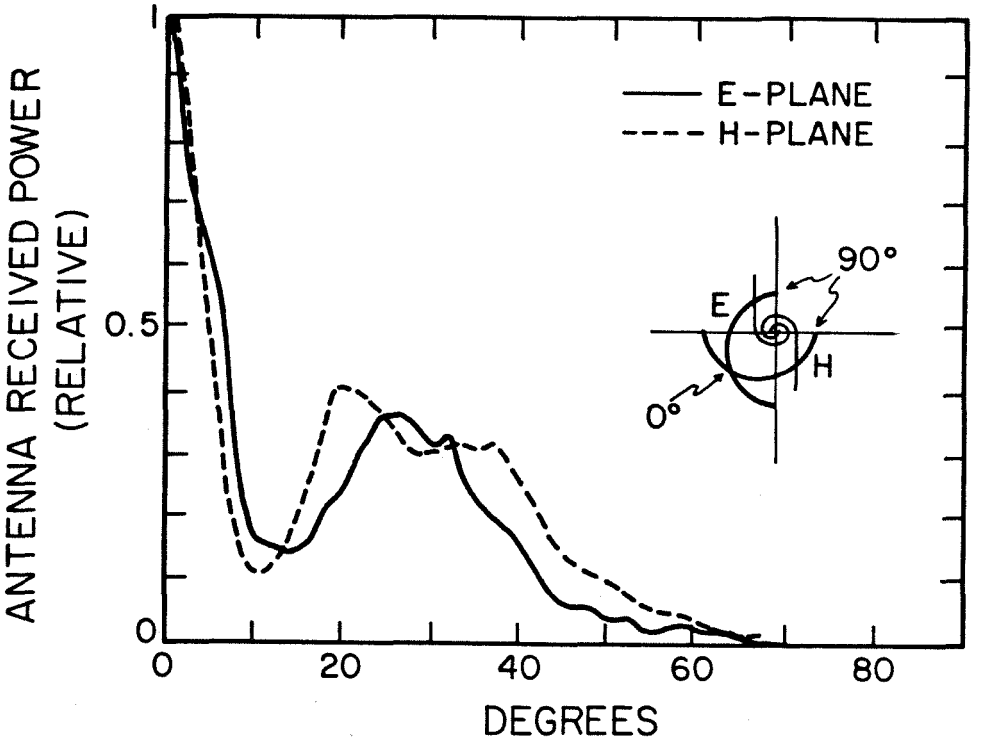

The efficiency of the spiral on dielectric

The optical set-up to measure the antenna efficiency is the same as that shown in Fig. 5, except that the collimator lens and the quarter-wave plate were removed. In order to ensure almost plane wave incidence onto the antenna, the distance between the objective lens and the horn was [11]

$$R > 2*D^2/\lambda$$

where D is the diameter of the lens

and λ is the free space wavelength.

The objective lens was a TPX [12] plano-convex lens 4.8 cm in diameter and 4.8 cm in focal length. The antenna was at the back side of the substrate lens. The substrate lens was an aplanatic lens. It was made of Dynasil 4000 fused quartz with a 1/2 inch radius. The input power of the antenna was assumed to be all the power incident on the objective lens. About 43% of the power was captured by the center antenna in Fig. 3 after focusing the optics, and no power registered in the two adjacent antennas. Since the antenna was circularly polarized and the incident wave was linearly polarized, the antenna could only capture half the incident power. Hence, if the incident wave was circularly polarized, the antenna efficiency should be 86%.

Bibliography

1. I. M. Hunter, "The Application of a Two Channel Circularly Polarized Radar to the Suppression of Rain Echoes." **Radar Research Establishment Journal**, vol. 36, pp. 1-37, 1955.

2. J. D. Dyson, "The Equiangular Spiral Antenna." **IRE Trans. Antennas Propagat.**, 7, pp. 181-187, 1959.

3. V. H. Rumsey, "Frequency Independent Antennas." **IRE Nat'l Convention Record, Pt. I**, pp. 114-118, 1957.

4. D. B. Rutledge and M. S. Muha, "Imaging antenna arrays." **IEEE Trans Antennas Propagat.**, AP-30, pp. 535-540, 1982.

5. J. D. Kraus and K. R. Carver, **Electromagnetics**, 2nd edition . New York, McGraw-Hill, Chpt. 14.

6. D. B. Rutledge, D. P. Neikirk, and D. P. Kasilingam, "Integrated Circuit Antennas". Series on **Infrared and Millimeter Waves**, vol. 10, Academic Press, New York.

7. M. Hatzakis, B. J. Canavello, and J. M. Shaw, "Single-step Optical Lift-off Process." **IBM J. Res. Develop.**, vol. 24, pp. 452-460, July 1980.

8. P. P. Tong, D. P. Neikirk, P. E. Young, W. A. Peebles, N. C. Luhmann,Jr., D. B. Rutledge, "Imaging polarimeter arrays for near-millimeter waves." **IEEE Trans. Microwave Theory Tech.**, vol. MTT-32, pp. 507-512, May 1984.

9. F. A. Jenkins and H. E. White, **Fundamentals of Optics**, 4th edition. New York, McGraw-Hill, 1976, Chpt. 9.

10. Ibid. Chpt. 27.

11. H. Jasik, **Antenna Engineering Handbook**, 1st edition, McGraw-Hill Book Company, 1961, Chpt. 34.

12. G. W. Chantry, J. W. Fleming, P. M. Smith, M. Cudby and H. A. Willis, "Far Infrared and Millimeter-wave Absorption Spectra of Some Low-loss Polymers." **Chem. Phys. Let.**, vol. 10, no. 4, pp. 473-477, August 1971.

4/TWO-DIMENSIONAL TRACKING ANTENNA ARRAY

This chapter describes a two-dimensional monolithic array that gives the elevation and azimuth of point source targets. The array is an arrangement of rows and columns of antennas and bismuth bolometer detectors on a fused quartz substrate. Energy is focused onto the array through a lens placed on the back side of the substrate. At 1.38 mm with a 50 mm diameter objective lens, the array has demonstrated a positioning accuracy of 26 arcminutes. In a differential mode this precision improves to 9 arcseconds, limited by the mechanics of the rotating stage. This tracking could be automated to a fast two-step procedure where a source is first located to the nearest row and column, and then precisely located by scanning. With signal processing the array should be able to track multiple sources.

The idea of the array

Tracking millimeter wave sources without scanning were done by a two dimensional monolithic array [1]. Figs. 1 and 2 show the array designed for wavelength of 1.2mm. Because of the series connection, the signal measured on the low-frequency leads gives the total power received along a particular row or column. The strongest column signal gives the source azimuth, and the strongest row signal gives the source elevation. More precise

Fig. 1. Tracking array. (a) View from the air side showing standard DIP package.

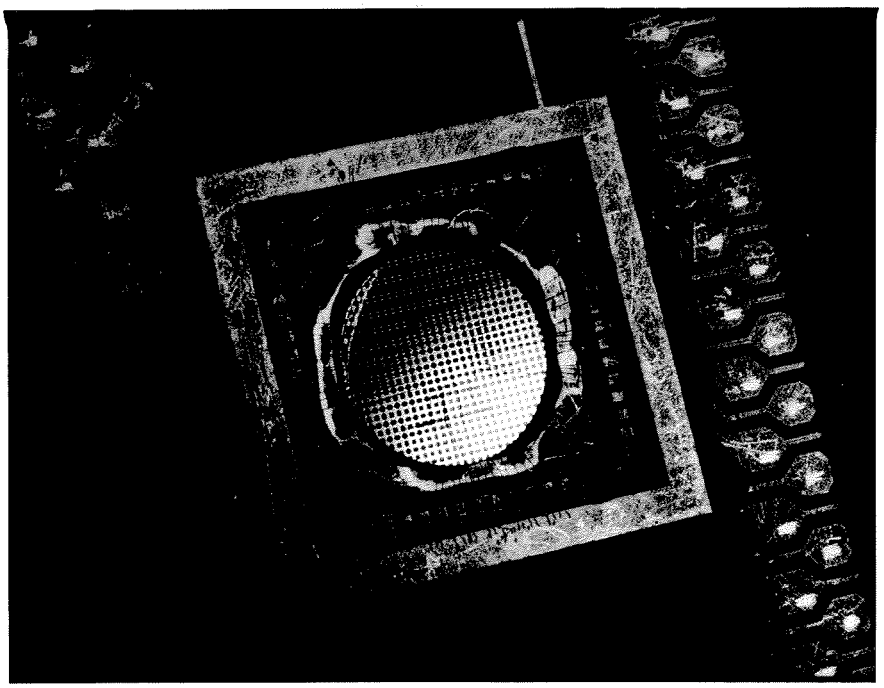

Fig. 1. Tracking array (b) View through substrate lens.

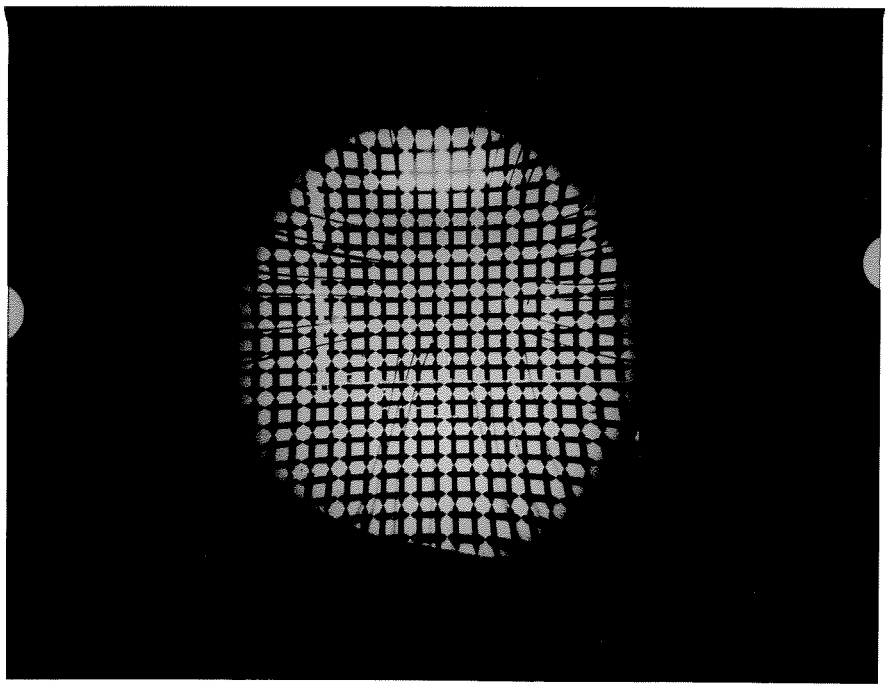

Fig. 2. Micrograph of a tracking array designed for 1.2 mm. The antennas are made of silver, and appear dark. The distance between adjacent rows (or columns) is 268 μm ($7/16\lambda_d$) and the distance between adjacent detectors in a single row or column is 535 μm ($7/8\lambda_d$). At its widest, the silver is 80 μm wide ($2/15\lambda_d$). Overlapping rows and columns are insulated from each other by a layer of polyimide.

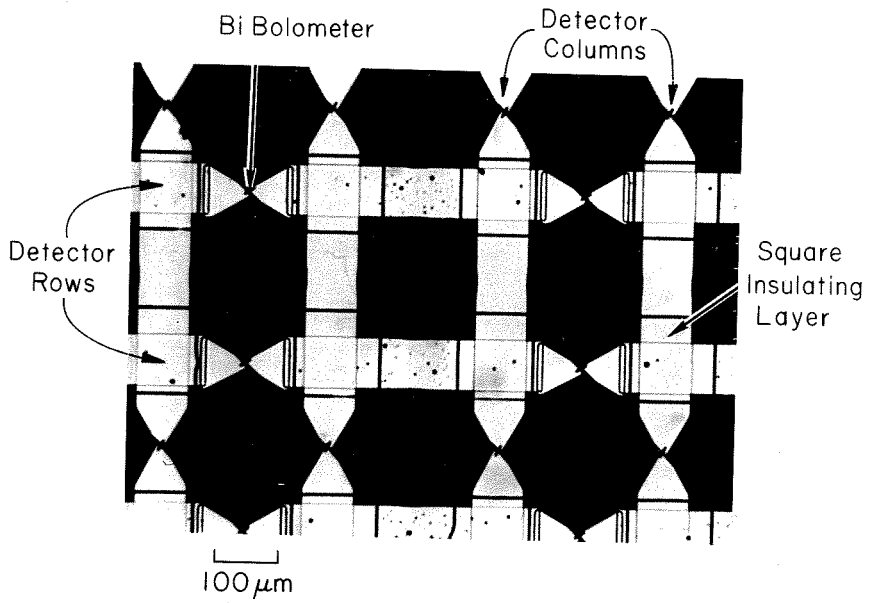

tracking information can be obtained by taking the difference between adjacent row and column signals in a way similar to optical centroid trackers [2] and microwave monopulse receivers [3]. In order to get this improvement, however, the array must be wobbled slightly to null the difference signal.

This array can locate a single source, and the question that naturally arises is: What happens when there are more point sources? If the sources all have different intensities, azimuths, and elevations, the array could track them simultaneously by identifying the row and column signals with equal magnitudes. If intensities, azimuths, or elevations are equal, there will be ambiguities. In a dynamic situation, these ambiguities may only persist for short periods of time, and with appropriate processing, multiple-target tracking should be feasible. It should also be possible to follow a single source when other sources pass through in the field of view of the array.

There is an interesting connection between the tracking array and X-ray transaxial tomographic imaging. The information produced by the array is the projections of the image along two perpendicular axes. The ambiguities that arise from sources of equal intensities, azimuths, and elevations could be resolved in principle by rotating the array about the optical axis to produce different projections. In some applications, such as missile guidance, the platform may rotate anyway. In principle, an arbitrary image can be reconstructed from its projections, similar to the way it is done in X-ray transaxial tomographic imaging [4].

The design, impedance and antenna patterns of the array

The array was designed by building large-scale microwave models. The model antennas were made of copper foil and the substrate was artificial dielectric with a dielectric constant of four to match the fused quartz substrates used at the millimeter wavelengths. The antennas were isolated from each other at low frequencies by masking tape. The spacing between rows and columns must be small enough so that the resolution does not degrade. A $\lambda_d/2$ spacing is adequate [5]. The dimensions were chosen by trial and error to give adequate impedance and radiation patterns.

The impedance of the model indicates the coupling efficiency for different kinds of detectors and the available bandwidth. Fig. 3 shows the model embedding impedance in ohms from 2 to 4 GHz. At the design frequency, 3 GHz, the impedance was 150 + j20 Ω. The resonance is weak, and this should be an adequate impedance for matching to either Schottky diodes or bolometers over a large bandwidth.

The radiation patterns of the array indicate how efficiently energy will be coupled into the array and also help determine the optical system. These patterns are needed because it is difficult to make accurate coupling efficiency measurements at millimeter wavelengths. Fig. 4 shows the radiation patterns into the substrate measured at a single detector in the array. The pattern for radiation into the air is at least 10 dB below the peak substrate power and is omitted. The patterns show a symmetrical beam with a half-power beamwidth of 30 degrees and the E-plane pattern shows large sidelobes that could not be eliminated.

Fig. 3. The impedance of the large-scale model of the antenna. It was plotted from 2 to 4 GHz on a Smith chart.

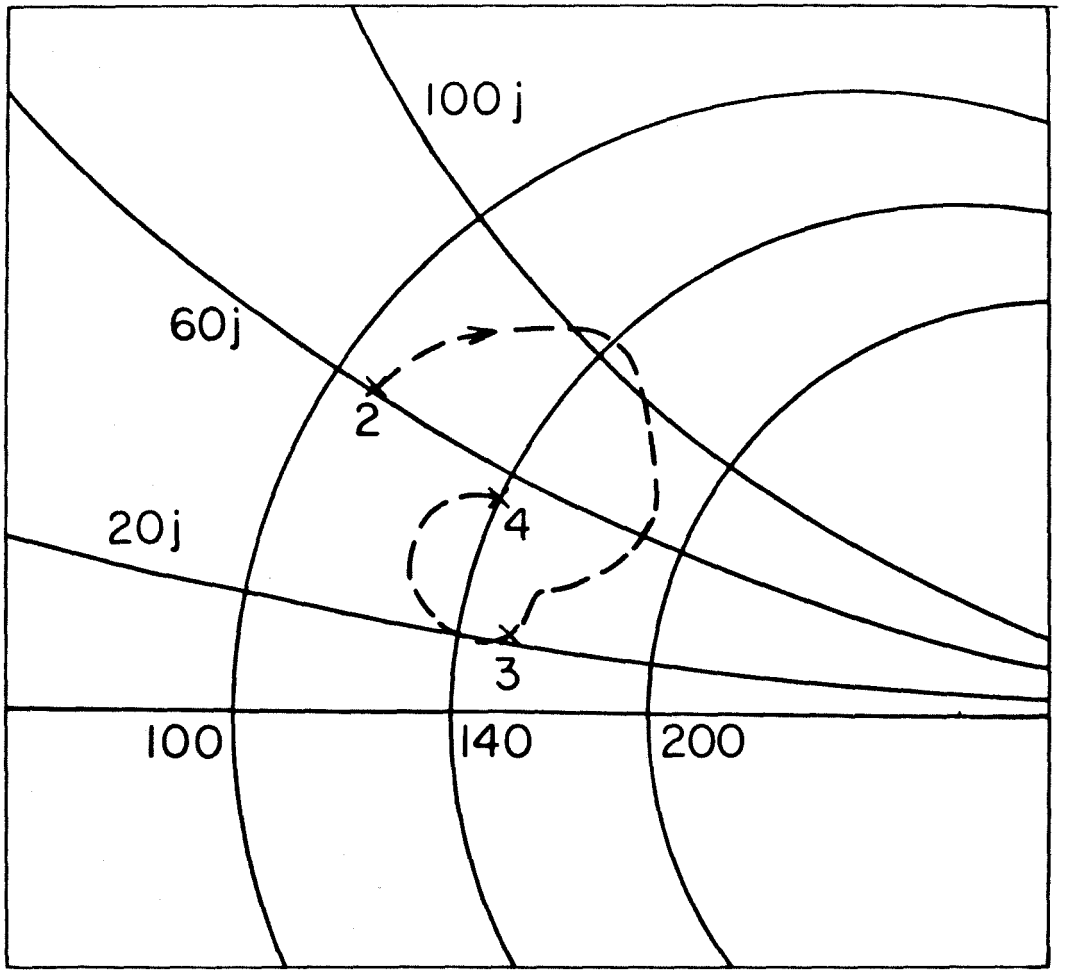

Fig. 4. Antenna patterns measured at a single detector diode at 10 GHz on a scale model. The plot is linear in power.

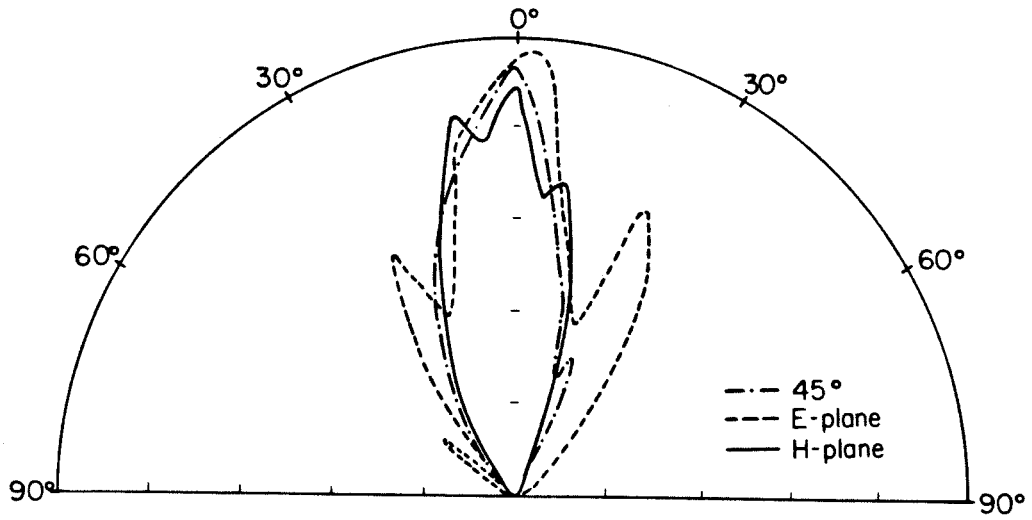

Integrated-circuit fabrication of the array

The array is made by conventional contact lithography and lift-off. The silver antennas were 80 nm thick. A half-micron polyimide insulating layer, Dupont Pyrallin 2555, was spun on between successive silver evaporations. Then 300 nm Bi bolometers were deposited. The particular array used in testing had bolometer resistances in the range 15 to 25 Ω. This is a poor match to the antenna but the resulting signal levels were sufficient to demonstrate the array properties. After fabrication, the array was mounted in a standard dual in-line package (DIP). The full array is 32 by 32, and this size can be adjusted during wire bonding. In our experiment the arrays were 7 by 7.

The number of antennas and detectors in a row or column affects the array sensitivity. This arrangement, where the output of a group antennas and detectors is combined, is called a multimode antenna [6]. A general property of multimode antennas is that the sensitivity degrades as the number of detectors increases. For the series-connected rows and columns, this is easy to understand because the total noise of a row or column is larger than the noise of a single detector. In terms of the noise equivalent power (NEP), for a row or column of n detectors, it is the square root of n times of the NEP of a single device. The NEP of the bolometers fabricated was about $10^{-9}W/(Hz)^{-1/2}$. Although an order of magnitude improvements in sensitivity can be achieved by the fabrication method shown in Chapter 2, the above sensitivity was already good enough in testing antennas and arrays.

The tracking of a target

Fig. 5 shows the optical set-up where the array was tested out in the submillimeter wavelength. The fused quartz substrate lens had a radius of curvature of 6.62 mm. It was an aplanatic lens [7]. The TPX [8] objective lens had a 70 mm focal length and a 50 mm diameter.

Fig. 6 shows the system patterns at 1.22 mm. The H-plane pattern is generated when the focused spot scans across a row. This pattern is sharply peaked, resembling the Airy pattern of the optical system [9]. The E-plane pattern results when the focused spot scans along a row from detector to detector. Ideally this signal should be constant, but Fig. 6 shows some roll-off, probably resulting from lens aberrations and differences in bolometers.

The next measurement demonstrated the tracking ability of the array. The source, a klystron at 1.38 mm, was translated in a plane 70 cm from the array. The power incident on the objective lens was 0.4 mW, and the output signal maxima were about 30 μV. The positions of the maxima were determined by standard sincfunction interpolation of sampling theory [10]. Fig. 7 compares the measured positions in the image plane with the predictions of geometrical optics. The average error in the image plane was 160 μm, and the corresponding error in the far field was 26 arcminutes. This is five times smaller than the diffraction-limited Rayleigh resolution limit for a pair of point sources. Much more precise tracking information can be obtained by taking the difference between adjacent row or column signals. As a function of angle, this pattern (Fig. 8) is the difference between two overlapping H-plane system patterns. It was measured with the differential inputs

Fig. 5. Substrate-lens coupled optical system.

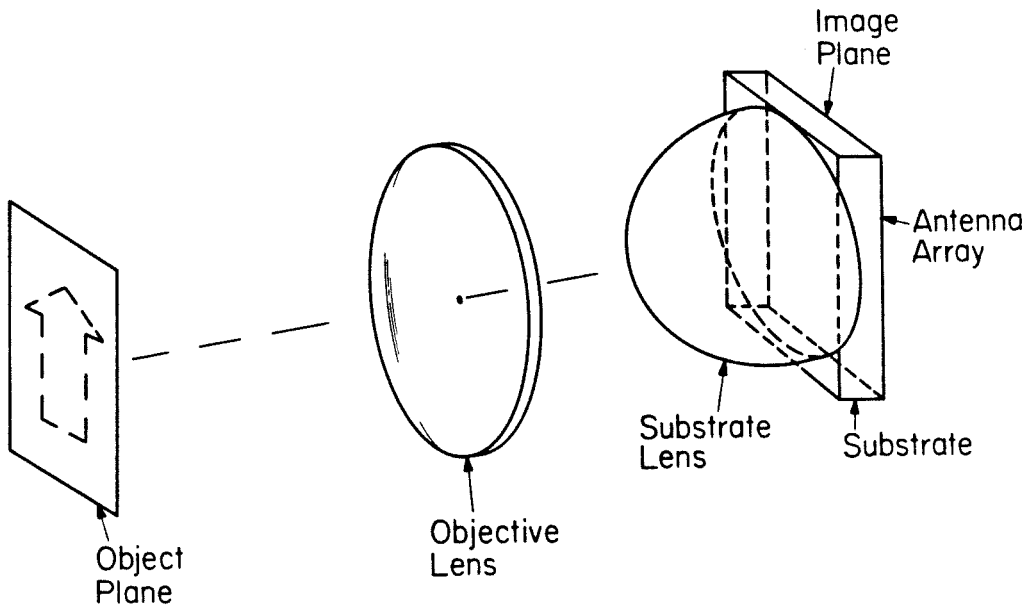

Fig. 6. Near-millimeter system patterns. The source was a CO_2-pumped C_{13} methyl-fluoride laser.

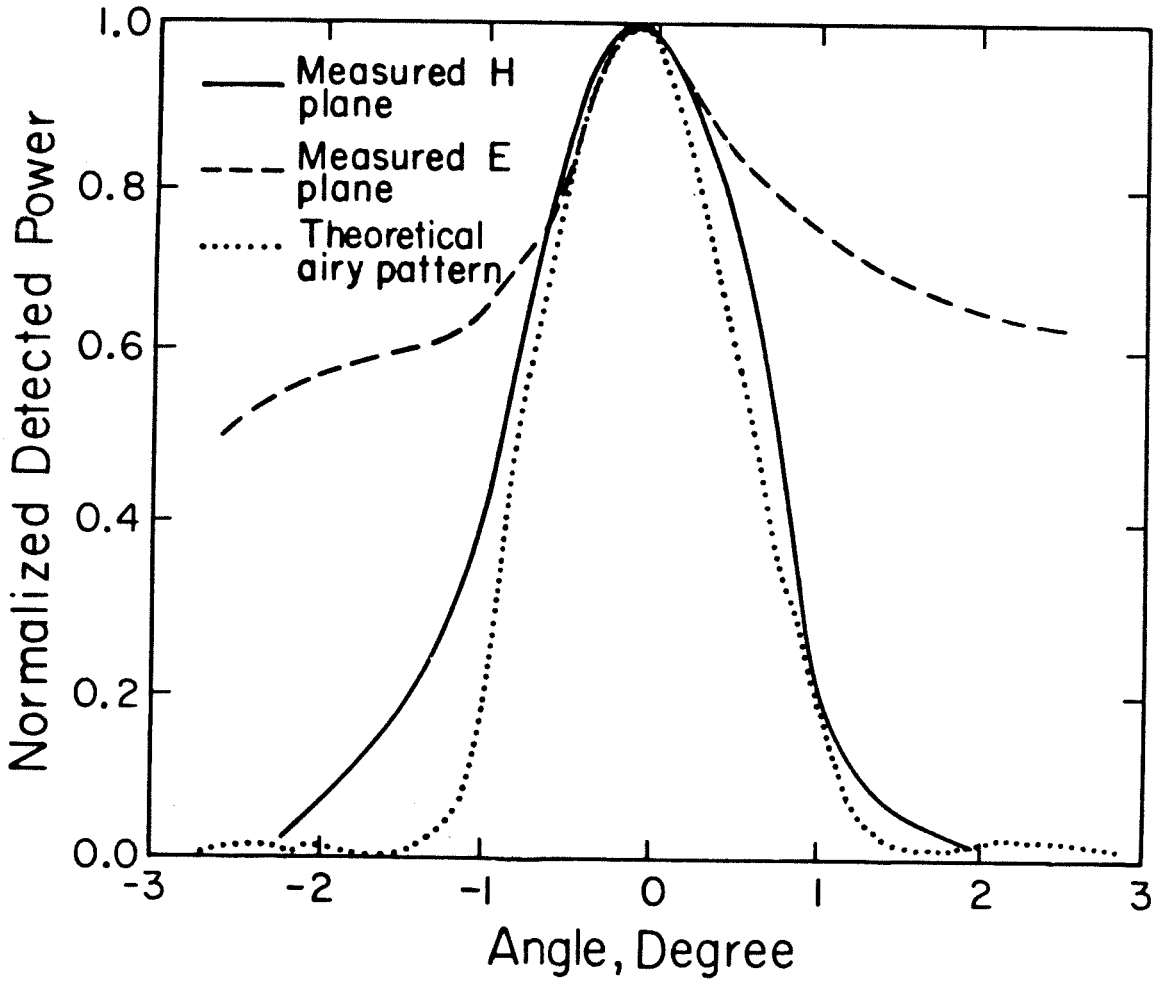

Fig. 7. Tracking demonstration. The grid shows the locations of the detector rows and columns.

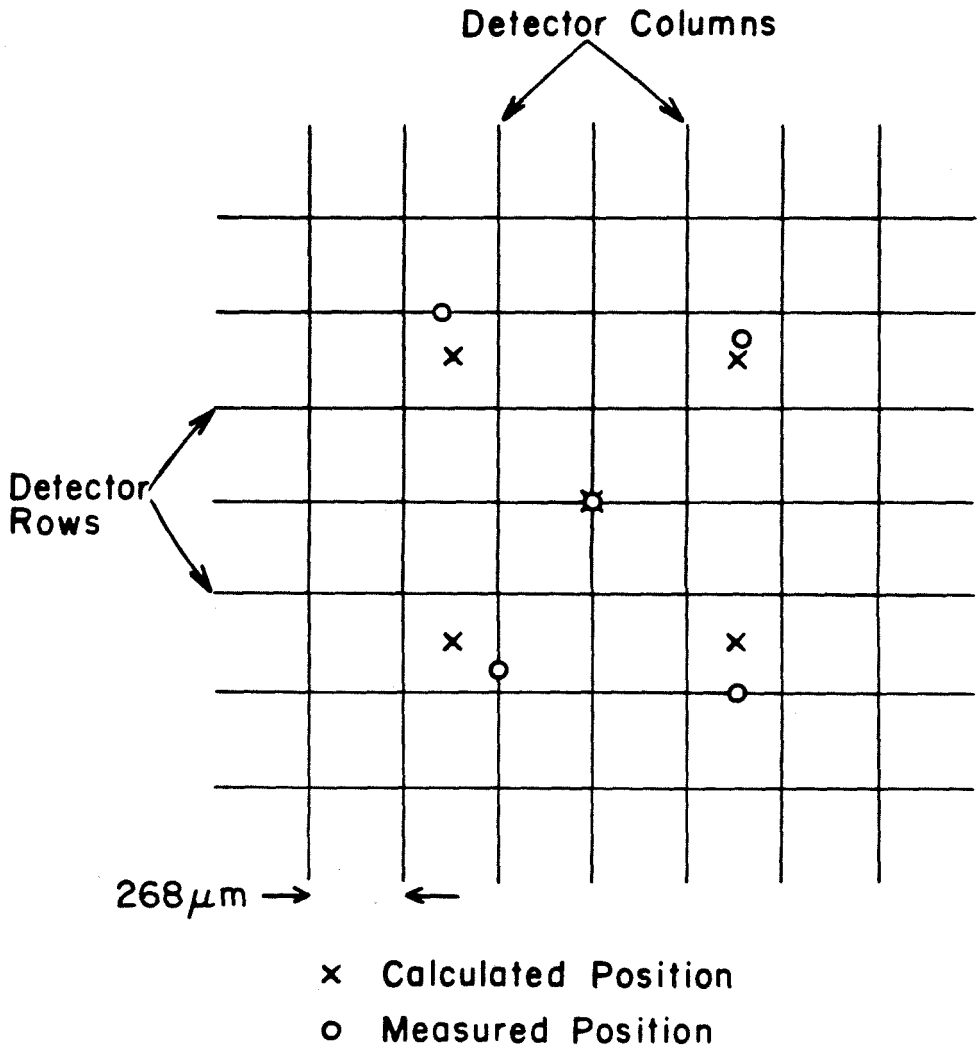

of a PAR-124 lock-in amplifier. The actual tracking procedure is similar to that of monopulse radars and optical centroid trackers where the system must be oriented to null the difference pattern. We were able to orient the system toward the source with an accuracy of 9 arcseconds, as indicated by the resulting difference signal. This accuracy was limited by the mechanics of the rotating stage rather than by the system signal-to noise ratio.

Fig. 8. Magnitude of the difference pattern of adjacent rows (ooo), along with the two overlapping H-plane system patterns (xxx and ●●●). The difference signal changes sign on each side of the null.

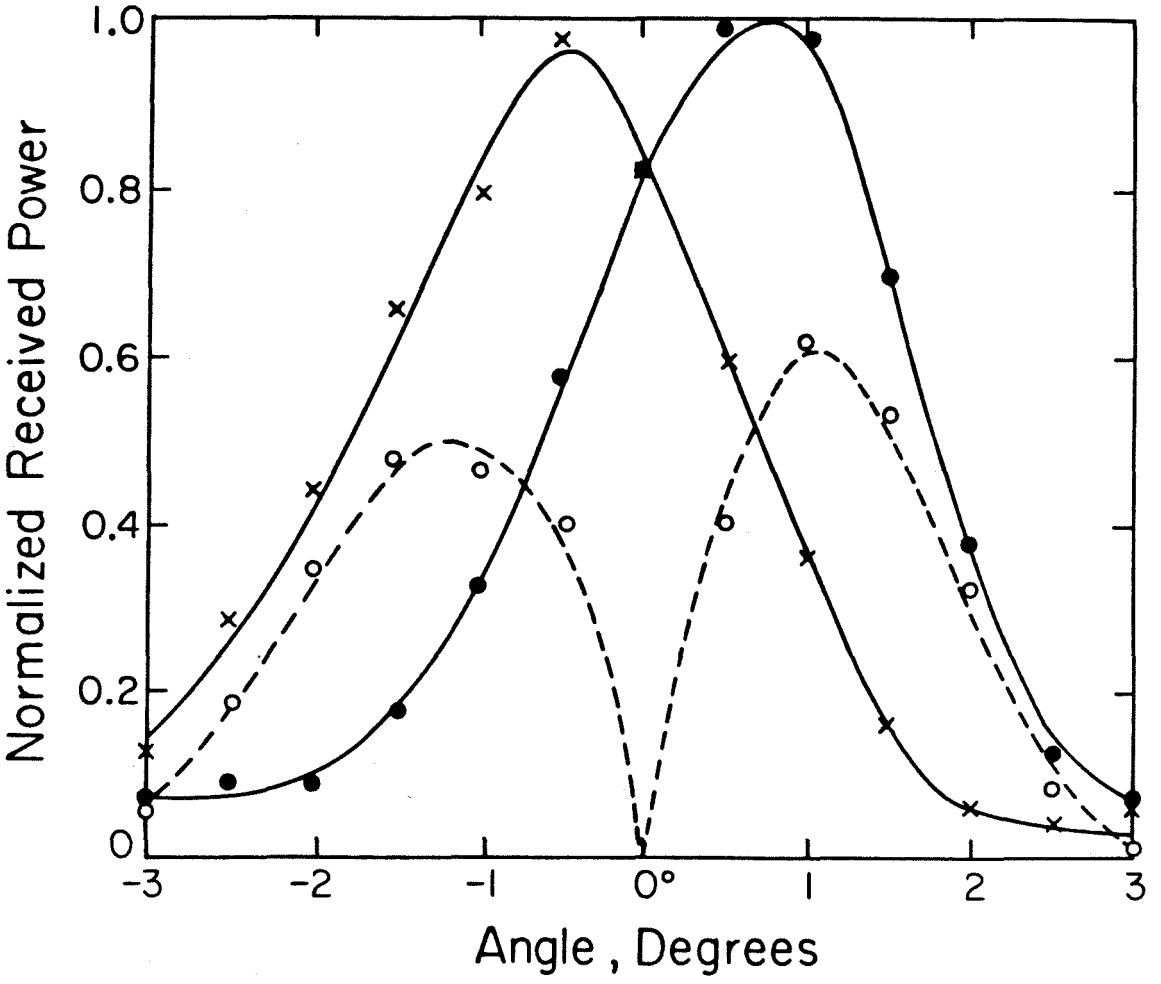

Bibliography

1. P. P. Tong, D. P. Neikirk, D. Psaltis, D. B. Rutledge, K. Wagner, P. E. Young, "Tracking Antenna Arrays for Near-Millimeter Waves." **IEEE Trans. Antennas and Propag.**, vol. 31, May 1983.

2. C. M. Crocker,Jr., "Wide Dynamic Range Instrument for Measurement of Laser Spot Position on Stationary and Moving Targets." **Proc. Soc. Photo-Opt. Instrum. Eng.**, vol. 255, pp. 69-72, 1980.

3. M. I. Skolnik, **Radar Handbook.** New York: McGraw-Hill, Chpt. 21, 1970.

4. H. Barrett and W. Swindell, "Analog Reconstruction Methods for Transaxial Tomography." **Proc. IEEE**, vol. 65, p. 89, 1977.

5. D. B. Rutledge, D. P. Neikirk, and D. P. Kasilingam, "Integrated Circuit Antennas." Series on **Infrared and Millimeter Waves**, vol. 10, Academic Press, New York.

6. D. B. Rutledge and S. E. Schwarz, "Planar Multimode Detector Arrays for Infrared and Millimeter-Wave Applications." **IEEE J. Quantum Electron.**, vol. 17, pp. 407-414, 1981.

7. F. A. Jenkins and H. E. White, **Fundamentals of Optics**, 4th edition. New York, McGraw-Hill, 1976, p. 567.

8. G. W. Chantry, J. W. Fleming, P. M. Smith, M. Cudby and H. A. Willis, "Far-infrared and Millimeter-wave

Absorption Spectra of Some Low-loss Polymers." **Chem. Phys. Let.**, vol. 10, no. 4, pp. 473-477, August 1971.

9. J. W. Goodman, **Introduction to Fourier Optics.** New York: McGraw-Hill, p. 64, 1968.

10. Ibid., pp. 21-25.

5/FUTURE WORK IN MILLIMETER WAVES

This thesis has presented the first linearly and circularly polarized antennas on dielectrics at millimeter wavelengths. The circularly polarized antennas can be put into arrays for polarization and intensity imaging. The idea will be similar to the linearly polarized antenna arrays except that now the antennas are right-handed and left-handed circularly polarized. Also the low-frequency lead can be removed without affecting the performance of the antenna. This is because, if the high frequency does propagate into the two vertical low frequency lines, then the antenna will not be circular. Biasing and the low-frequency power detection can be done directly at the end of the spiral. This will make the antenna more compact and will allow two-dimensional imaging.

Another interesting area will be combining both the linearly and circularly polarized antennas in an array. If the array works, then, through power detection alone, the array could detect the components of the electric field and the phase between them. That means there is no need to detect the phase between the electric fields directly. That simplifies the measurement procedures and set-up.

This thesis has also presented the first two-dimensional

tracking antenna array. This array images point targets. For general targets, it would be best if output from each individual detector can be extracted. Now we are limited by the amount of electrical wires that can go to individual detectors. The scheme to get around using wires would be to have a 2-dimensional array of spiral antennas without low frequency leads, all of them are separated from one another. Thermocouples are the detectors. Signals can be coupled out by two different methods. One is to integrate amplifiers and light emitting diodes to the detectors. Then, instead of electrical outputs, one would have optical output. Another method would be to bring an array of probes in from the back side onto the array, a separate probe for each of the spiral end to couple the signal out. A general two-dimensional imager will be possible by either of the above methods.

Also of interest will be integrating sources such as IMPATT or GUNN diodes instead of detectors into the arrays of integrated circuit antennas. We have developed some very low-impedance narrow-band antennas for impedance matching in this application.

APP1/THE RESPONSE OF ANY POLARIZED ANTENNA TO ANY POLARIZED WAVE

This appendix addresses the response of any polarized antenna to any polarized wave. The experimental work was done at millimeter wavelengths. Modified bow-tie antenna is the linearly polarized antenna; equiangular spiral antennas are the elliptically and circularly polarized antennas. The experimental results match with theory.

The linearly, elliptically and circularly polarized antennas

Linearly, elliptically and circularly polarized antennas are used. They are integrated-circuit antennas on a dielectric material. Modified bow-tie antennas are the linearly polarized antennas [1]. Fig. 1 is a drawing of a few of them designed for a fused-quartz substrate. Bismuth bolometers are the detectors. Fig. 2 is a photograph of an array of them in a package. The array was designed at 375 GHz in frequency or 0.8 mm in wavelength. All the antennas are linearly polarized with an axial ratio (definition in the Chapter 2) more than 140. Chapter 2 gives a more elaborate explanation of the antenna. Equiangular spiral antennas [2] are the

Fig. 1. Linearly polarized modified bow-tie antennas designed for use on a fused-quartz substrate ($\varepsilon_r = 4$).

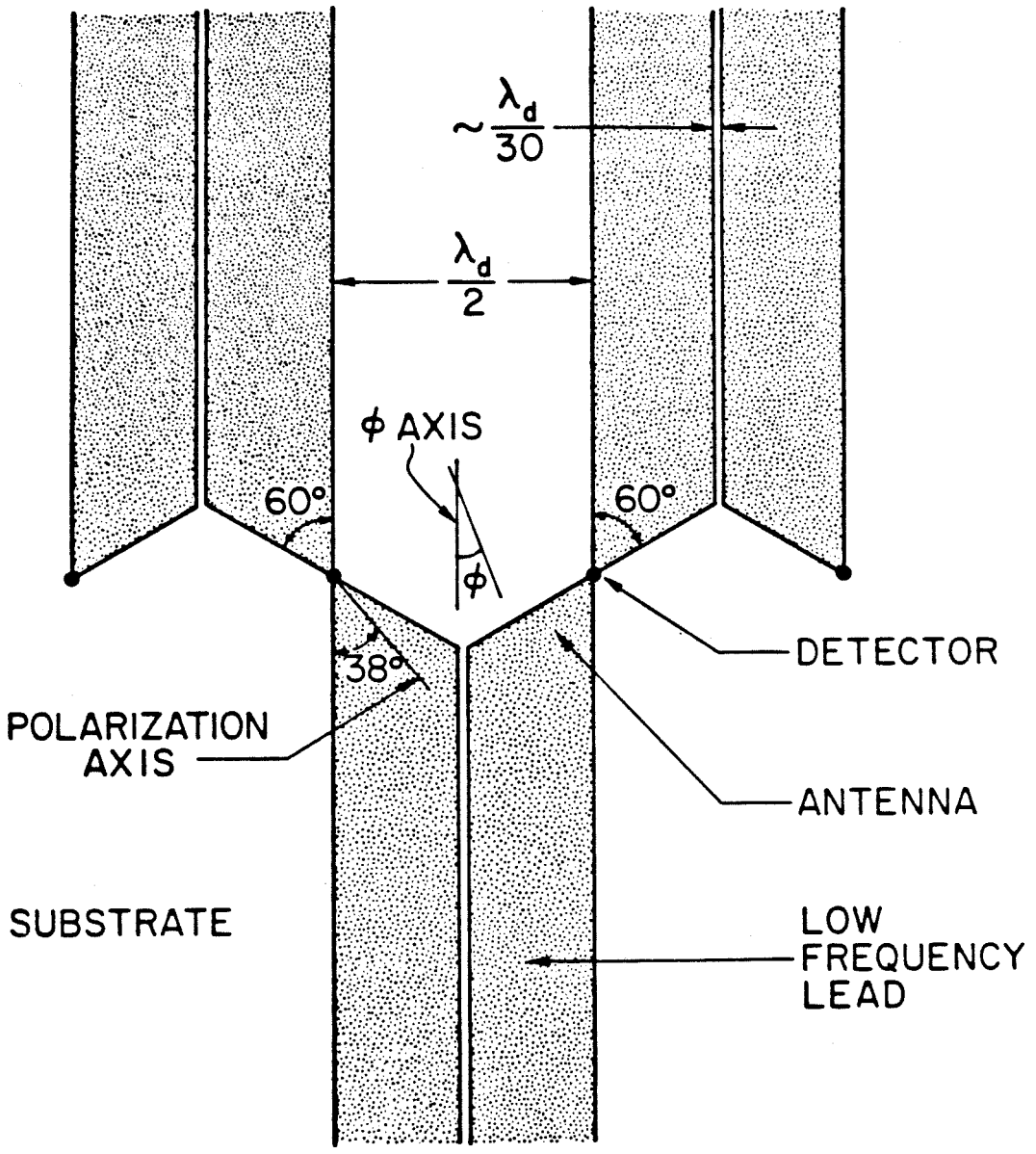

Fig. 2. Linearly polarized antenna array in a standard DIP package.

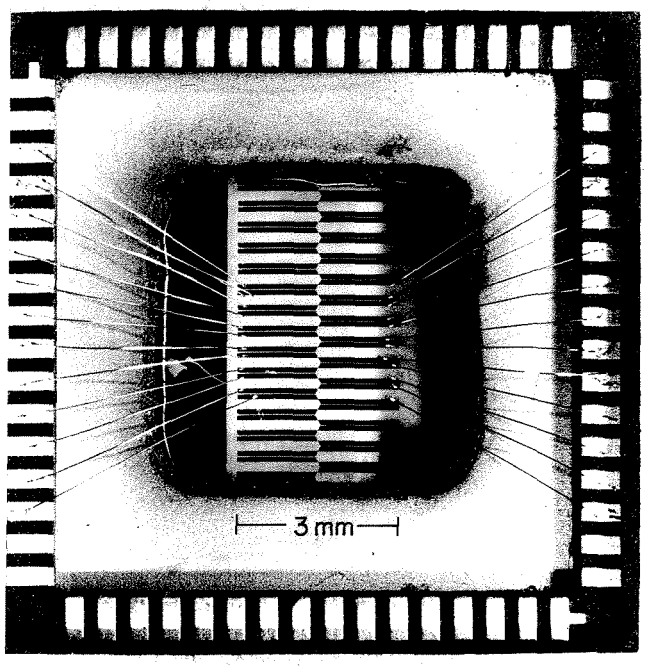

elliptically and circularly polarized antennas. Fig. 3 is a drawing of a circularly polarized antenna. It is a self-complementary antenna [3]. Again Bi bolometer is the detector. Fig. 4 is a photograph of a few of the antennas in a package. Two are right-hand circularly polarized and the center one is left-hand circular. It was designed at 94 GHz or 3.2 mm with an axial ratio less than 1.2. Chapter 3 discusses this antenna further. The antenna becomes elliptical when there is insufficient spiral length or the detector position occupies a relatively large area. Fig. 5 shows the photograph of an array of elliptically polarized antennas at 94 GHz in a package.

The generation of elliptically polarized waves

Fig. 6 shows the set-up to generate a linearly polarized wave at any orientation. A linearly polarized wave at 375 GHz coming out of the open-ended waveguide through the polarizer was collimated by the lens. The wave passing through the half-wave plate was received by the modified bow-tie antennas at the back of the substrate lens. A half-wave plate is an anisotropic uniaxial material [4]. The axes parallel and perpendicular to theopticalaxis have a slightly different dielectric constant. In our case it was made up of crystal quartz. The half-wave plate could rotate the electric field of the incident linearly polarized wave from 0 to 180 degrees. It was then picked up by antennas at the back of the substrate lens.

Fig. 7 is a picture showing the set-up to generate a wave of any ellipticity or axial ratio. Linearly polarized waves at 94 GHz coming out of a horn were collimated by a lens. The wave was electronically

Fig. 3. Circularly polarized equiangular spiral antenna designed for use on a fused-quartz substrate ($\varepsilon_r = 4$).

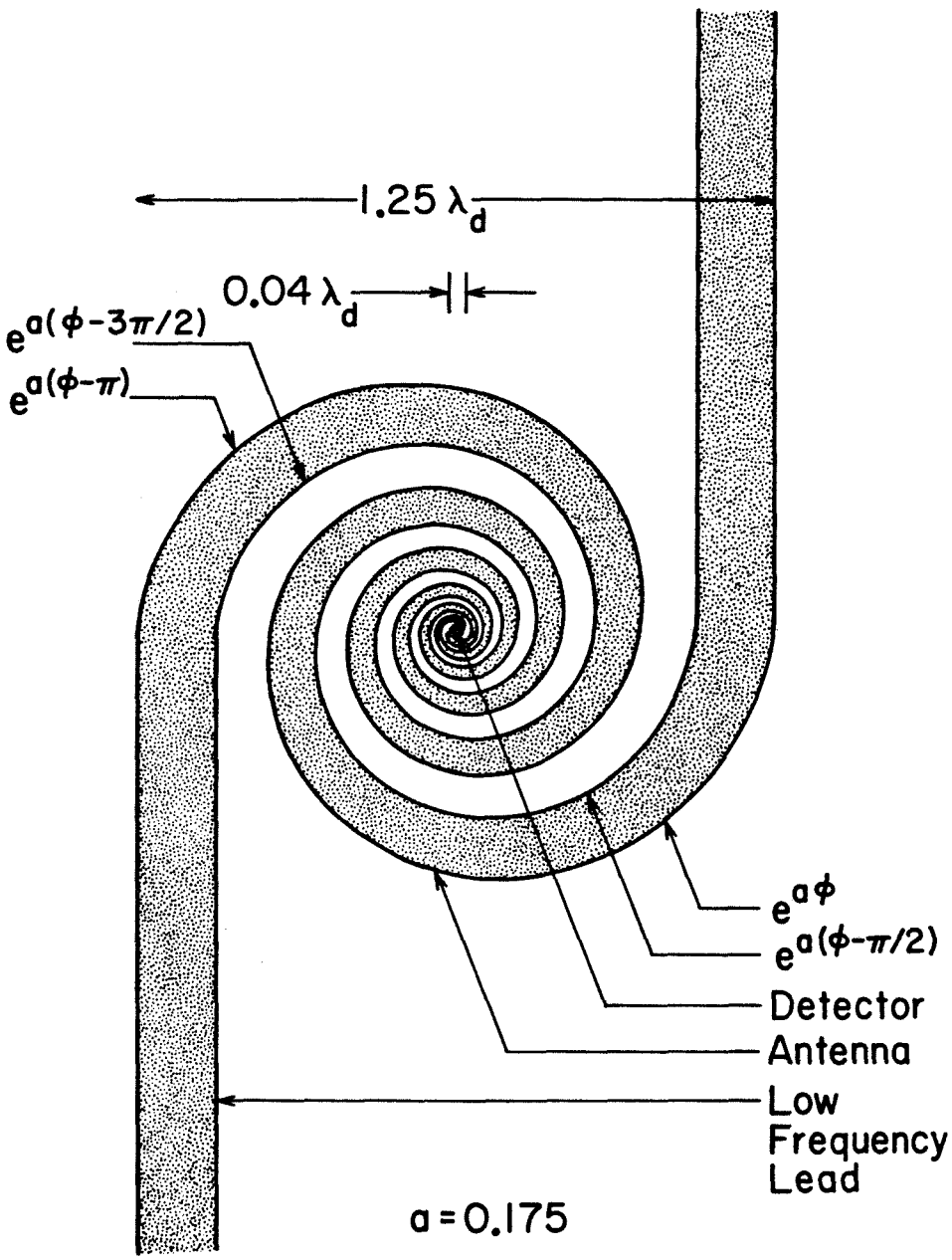

Fig. 4. Circularly polarized antenna array in a DIP package.

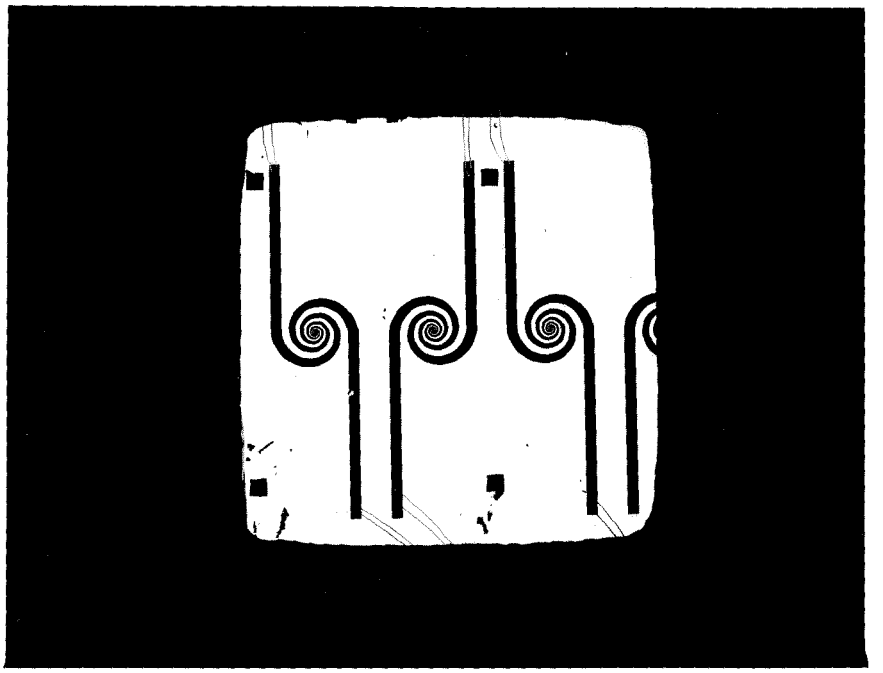

Fig. 5. Elliptically polarized antenna array in a DIP package.

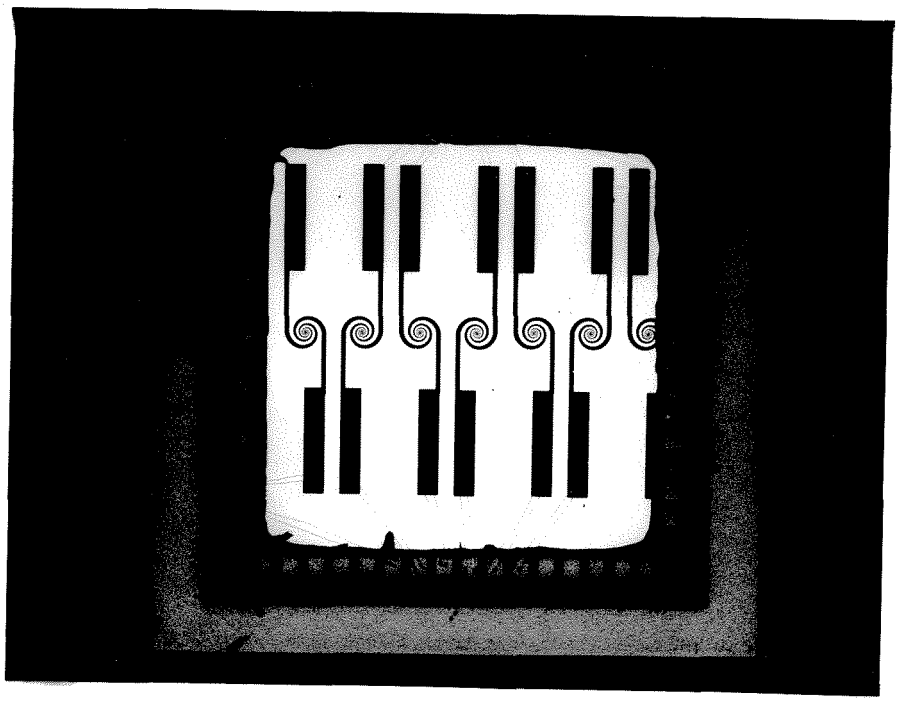

Fig. 6. Optical set-up to test the response of linearly polarized antennas to linearly polarized wave.

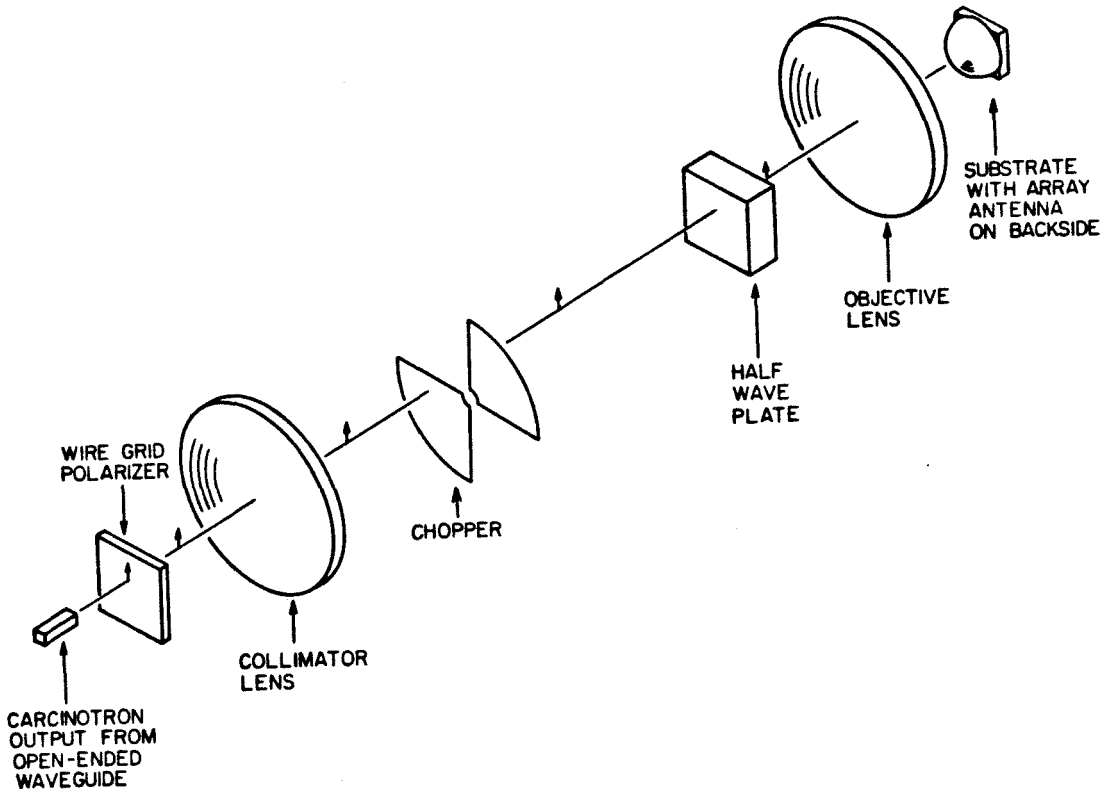

modulated at 1 kHz. It then passed through a quarter-wave plate and an objective lens and received by antennas at the back of a substrate lens. Quarter-wave plate is like half-wave plate except that it is half its thickness. Depending on its orientation, it changes a linearly polarized wave from linear to elliptical to circular wave.

The theoretical and experimental responses of the antennas to the waves

The power received by any polarized antenna to any type of polarized wave was proportional to [5] :

$$P_r \propto |E_t^* \hat{E}_r|^2 \qquad (1)$$

where E_t is the incident electric field vector
and $\hat{E}_r$ is the electric field excited by the antenna if it is transmitting. It is a unit vector.
Both can be represented by Jones vectors [6].

The incident electric field is a linearly polarized wave going through either a half-wave or a quarter-wave plate. Linearly polarized wave is represented as

$$\begin{bmatrix} 0 \\ 1 \end{bmatrix}. \qquad (2)$$

The effect of the uniaxial crystal can be represented by

$$\begin{bmatrix} \cos\theta & -\sin\theta \\ \sin\theta & \cos\theta \end{bmatrix} \begin{bmatrix} 1 & 0 \\ 0 & e^{i\phi} \end{bmatrix} \begin{bmatrix} \cos\theta & \sin\theta \\ -\sin\theta & \cos\theta \end{bmatrix} \qquad (3)$$

where θ is the angle between the optical axis and the direction perpendicular to the linearly polarized wave

Fig. 7. Optical set-up to test the response of both the elliptically and circularly polarized antennas to elliptically polarized wave.

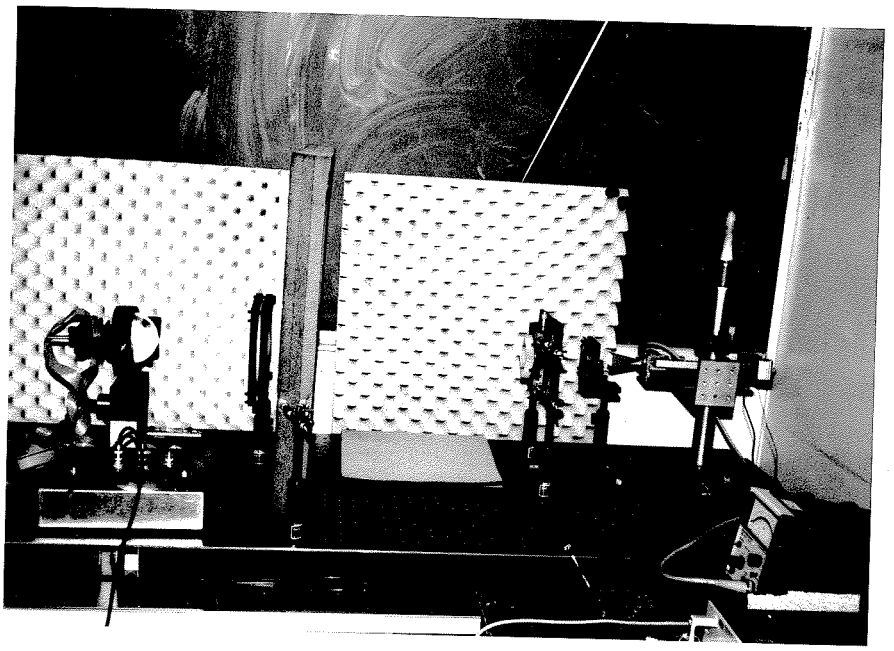

as shown in Fig. 8, and ϕ represents the amount of anisotropy of the crystal
--for quarter-wave plate, it is 90 degrees;
for half-wave plate, it is 180 degrees.

Now $\hat{E}_r$, the antenna effect, is

$$\begin{bmatrix} 1 \\ \delta e^{i\gamma} \end{bmatrix} \times (1 + \delta^2)^{-1/2} \qquad (4)$$

for linearly polarized antenna: $\delta = 0$ or infinite
and $\gamma = 0$

for circularly polarized antenna: $\delta = 1$
and $\gamma = \pm\pi/2$.

Putting equations 2,3,4 into 1 to get equation 5:

$$P_r \propto \sin^2 2\theta(1-\cos\phi)/2+$$

$$\delta(\sin 2\theta \sin^2\theta(\cos\gamma-\cos(\phi-\gamma))+$$

$$\sin 2\theta\cos^2\theta(\cos(\phi+\gamma)(1-\cos\phi)-\sin(\phi+\gamma)\sin\phi))+$$

$$\delta^2(1+(\sin^2 2\theta/2)(-1+\cos\gamma\cos(\gamma+\phi)+\sin\gamma\sin(\gamma+\phi)).$$

Equation 5 will be studied under three different conditions and verified by experiments. The three conditions all involved linearly polarized wave going through different uniaxial crystals and they are:
(1). The response of a linear antenna to a linearly polarized wave with any orientation. A half-wave plate was used.
(2). The response of a circular antenna to an elliptical wave. A quarter-wave plate was used.
(3). The response of an elliptical antenna to an elliptical wave.

Fig. 8. The relationship between the incident electric field direction and the orientation of the uniaxial crystal.

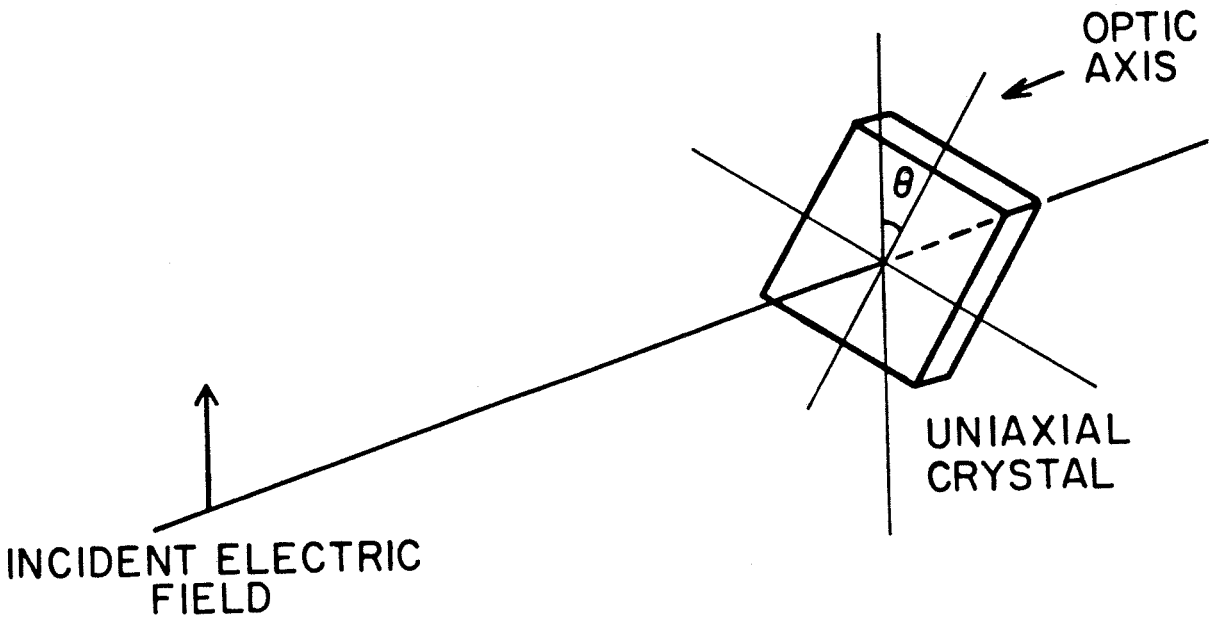

Condition 1 :

When the antenna is linear :

$$P_r \propto 1-\sin^2 2\theta(1-\cos\phi)/2.$$

If the uniaxial crystal has the exact thickness of a half-wave plate or ϕ = 180 degrees, then

$$P_r \propto \cos^2 2\theta.$$

Fig. 9 shows the experimental and theoretical results. The experiment was done using the set-up in Fig. 6 with the antenna shown in Fig. 2 and at 375 GHz. In the millimeter wave area, the dielectric constants of materials sometimes are not well tabulated. So it would be difficult to know the exact thickness to make a half-wave plate or to make ϕ exactly 180 degrees. But from the theory, even if ϕ is 160 degrees, the response of the linearly polarized antenna will not be much affected.

Condition 2:

When the antenna is circular, with $\gamma = \pi/2$,

$$P_r \propto 1-\sin 2\theta \sin\phi.$$

If the uniaxial crystal has the exact thickness of a quarter-wave plate or ϕ = 90 degrees, then

$$P_r \propto 1-\sin 2\theta.$$

Fig. 10 shows the theoretical and experimental results. The experimental work was done using the set-up in Fig. 7 and with the antenna shown in Fig. 4 and at 94 GHz. With ϕ = 110 degrees, the antenna response is still not

Fig. 9. The theoretical and experimental response of a linearly polarized antenna in the set-up shown in Fig. 6.

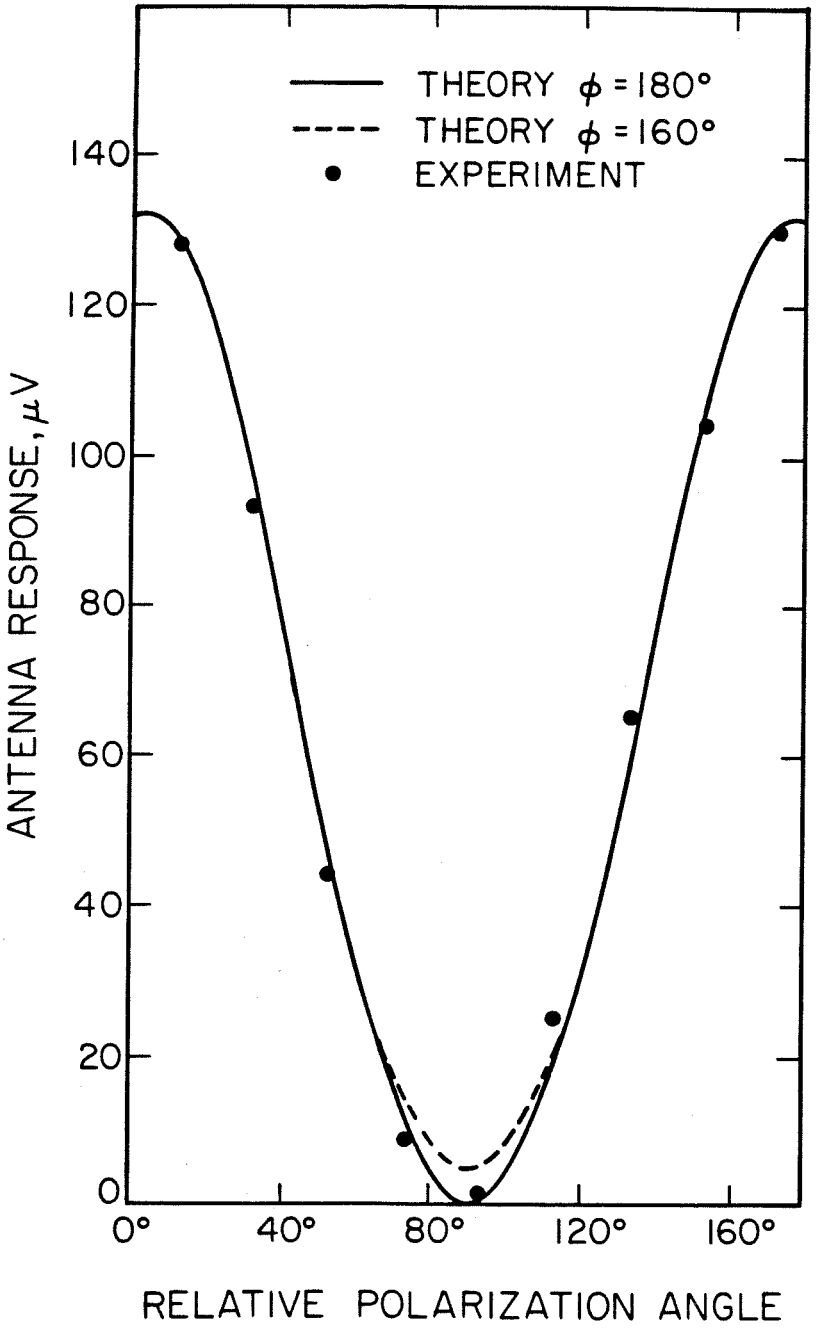

Fig. 10. The theoretical and experimental response of a circularly polarized antenna in the set-up shown in Fig. 7.

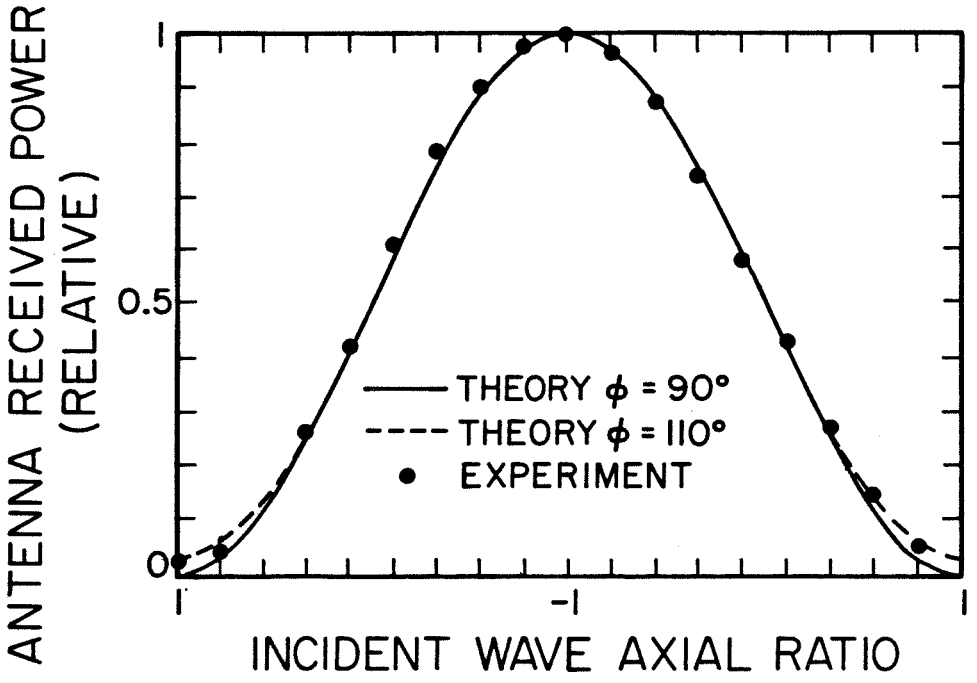

much affected.

Condition 3:

When the antenna is elliptically polarized and the uniaxial crystal has the exact thickness of a quarter-wave plate, then

$$P_r \propto \sin^2 2\theta(1-\delta^2)/2+$$

$$\delta^2-\delta\sin 2\theta(\sin\gamma+\cos\gamma\cos 2\theta).$$

Fig. 5 and Fig. 7 show the antenna and the set-up used for the experiment done at 94 GHz. The experimental points fit the theory if γ = 75 degrees and δ = 0.8 in equation 4. Fig. 11 shows the theoretical and experimental results.

This chapter studies the response of any polarized antennas to any polarized waves. Experiments have been done in the millimeter wavelength. Results are close to theory.

Fig. 11. The theoretical and experimental response of an elliptically polarized antenna in the set-up shown in Fig. 7.

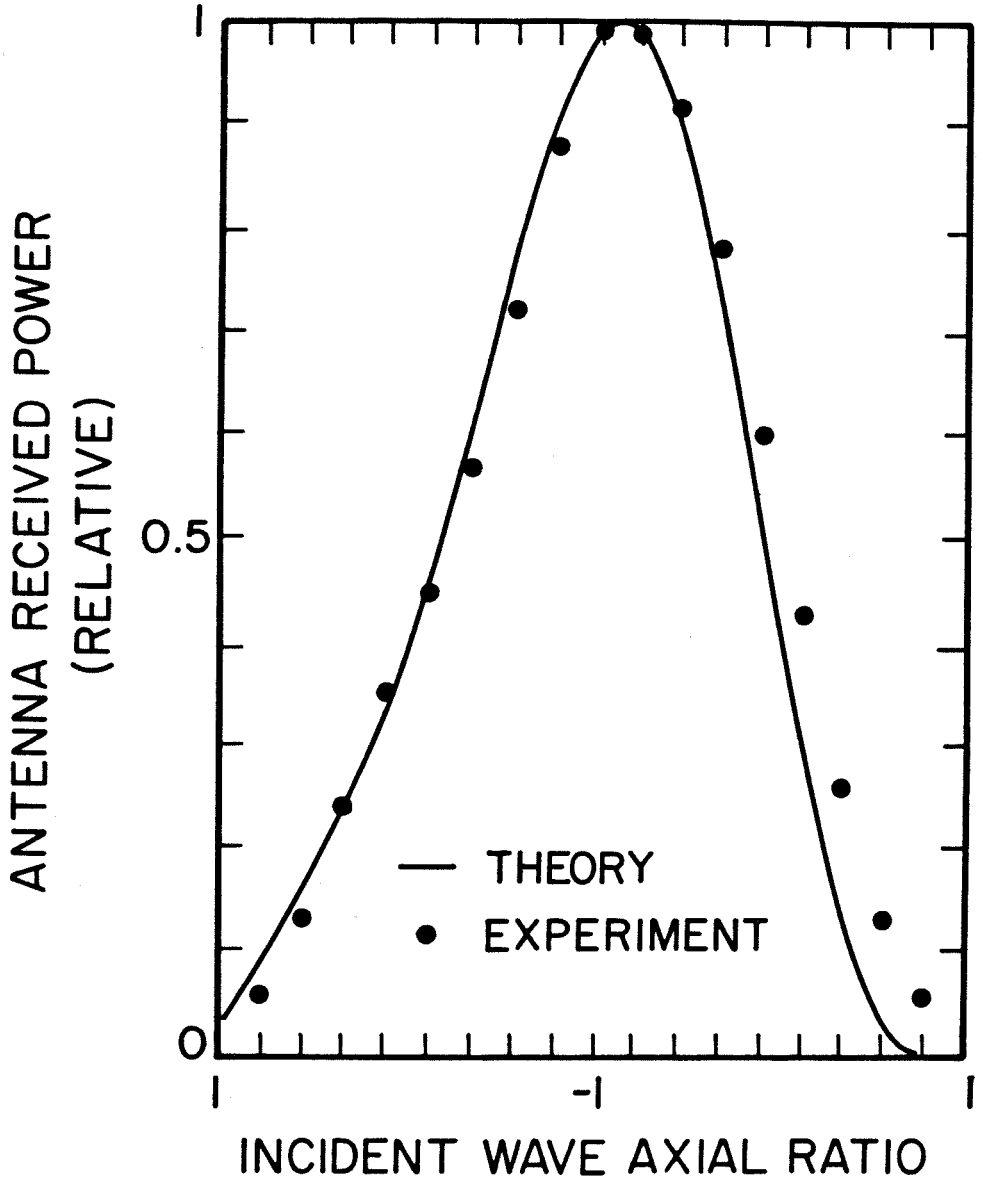

Bibliography

1. P. P. Tong, D. P. Neikirk, P. E. Young, W. A. Peebles, N. C. Luhmann,Jr., D. B. Rutledge, "Imaging polarimeter arrays for near-millimeter waves." **IEEE Trans. Microwave Theory Tech.**, vol. MTT-32, pp. 507-512, May 1984.

2. J. D. Dyson, "The Equiangular Spiral Antenna." **IRE Trans. Antennas Propagat.**, vol. 7, pp. 181-187, 1959.

3. J. D. Kraus and K. R. Carver, **Electromagnetics**, 2nd edition . New York, McGraw-Hill, Chpt. 14.

4. F. A. Jenkins and H. E. White, **Fundamentals of Optics**, 4th edition. New York, McGraw-Hill, 1976, p. 567.

5. Y. C. Yeh, "The Received Power of a Receiving Antenna and the Criteria for its Design." **Proc. of IRE**, pp. 155-158, 1949.

6. E. Hecht and A. Zajac, **Optics**, 4th edition. Addison-Wesley, Chpt. 8.

APP2/THE ANTENNA PATTERNS OF A LONG WIRE ANTENNA

This appendix describes the antenna patterns of a long wire antenna on a dielectric at 94 GHz. Both theory and experiments will be shown.

Fig. 1 is a photograph of a long wire antenna on a dielectric in a DIP package. Its width is 20 μm and its length is slightly more than $6\lambda_d$. Fig. 2 shows the tip of the antenna. The part of the line that is bright is silver. The rough part is bismuth on silver while the bolometer detector is at the position as shown. The patterns of this antenna were measured at 94 GHz by the methods and set-up as described in Chapter 3.

The theoretical and experimental H-plane patterns

The theoretical H-plane or the plane with a transverse electric field or the ϕ direction in the spherical co-ordinate has already been done [1]. It was plotted out on Fig. 3 together with the experimental results for quartz substrate. The experimental results were close tothe theory. This, in fact, tested out the methods and set-up for this antenna pattern measurement technique.

Fig. 1. A long wire antenna on a dielectric in a DIP package.

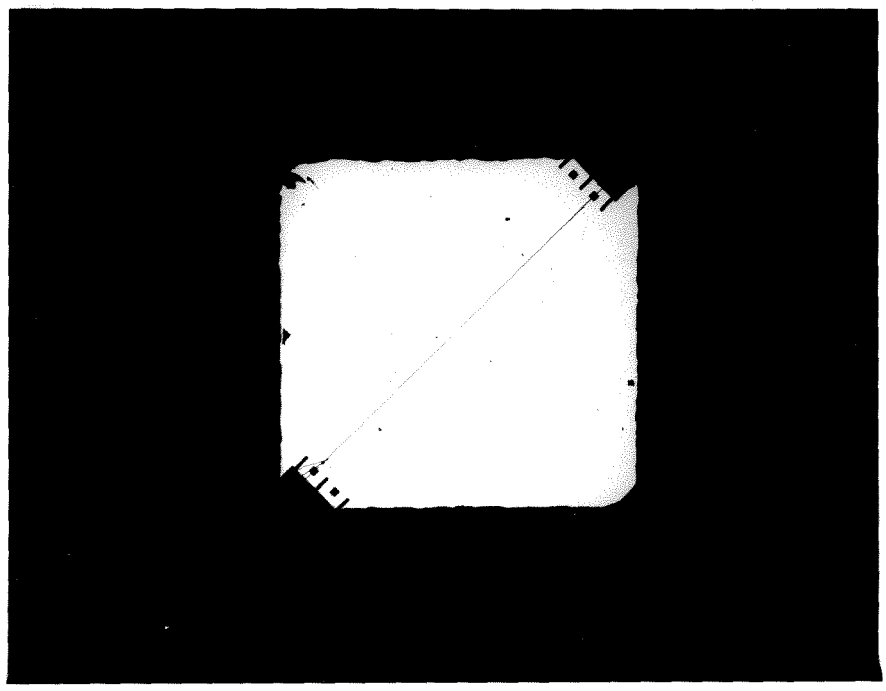

Fig. 2. The tip of the long wire antenna. The bright line is silver. The rugged surface is bismuth on silver while the bismuth bolometer is at the position as shown.

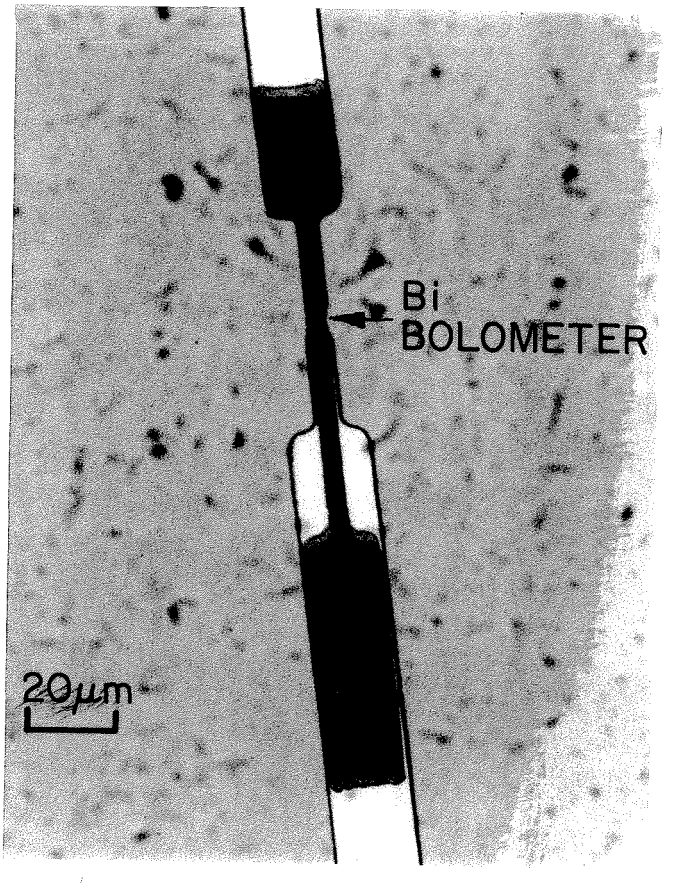

Fig. 3. The antenna patterns of a long wire antenna on dielectric. Only the patterns on the dielectric side are shown. The power radiated into the air side is at least 10 dB down.

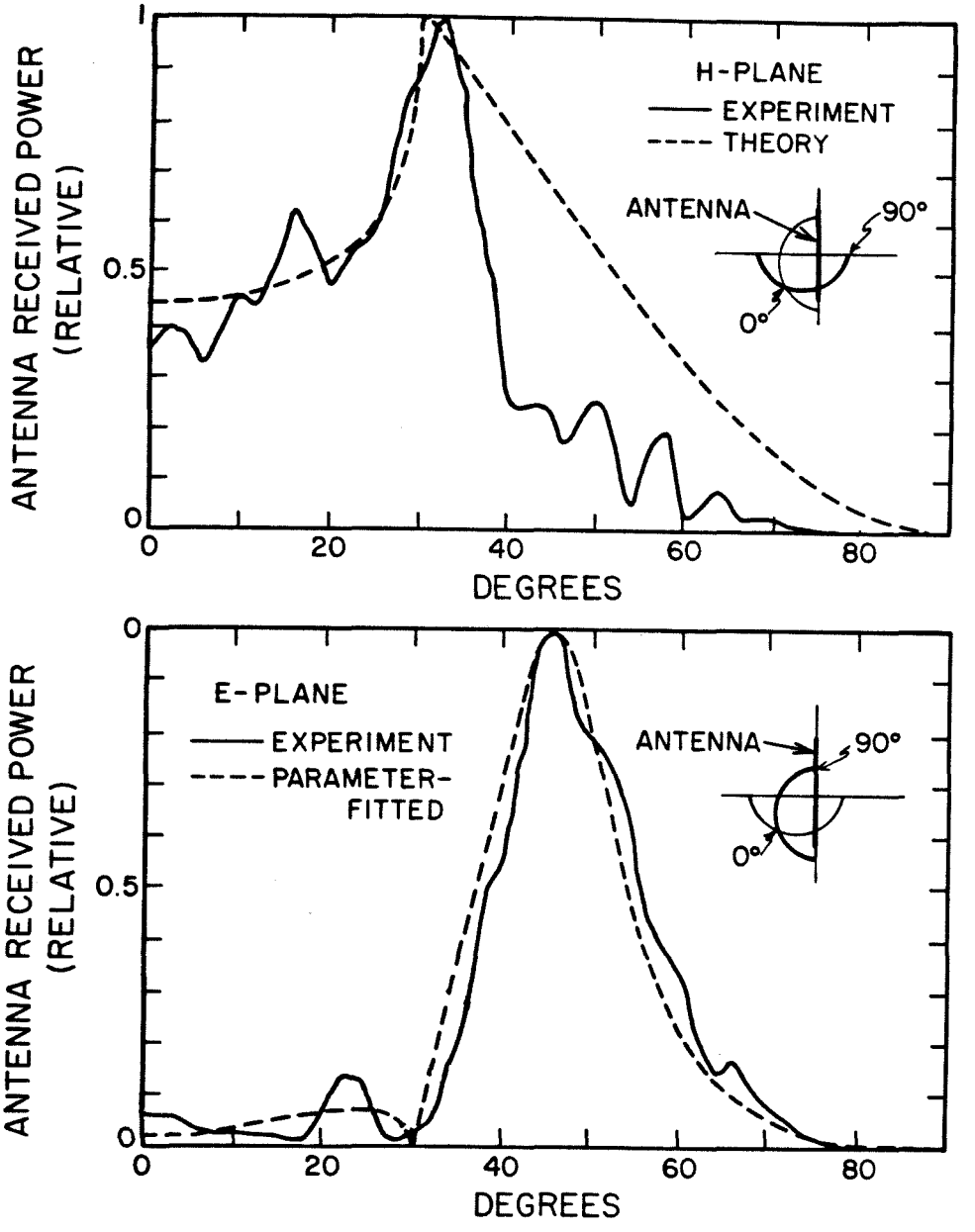

The experimental and parameter-fitted E-plane pattern

The E-plane pattern or the plane with a transverse magnetic field or the θ direction in the spherical co-ordinate of a long wire antenna on a dielectric will be shown below. The current along the wire is assumed to be of the forms:

$$I = C\exp(-\alpha z - j\beta z).$$

The far field E-plane radiation intensity of this current radiating into a material of dielectric constant n is proportional to [2]:

$$K = | 1/((\alpha/k)-j(n\sin\theta-\beta)) |^2$$

with k as the free space wave number.

The far field radiation intensity of this current on a dielectric material will be proportional to K multiplying the dipole radiation pattern on a dielectric [3].

For $0 < \theta <$ the critical angle, it is proportional to :

$$K \times M\cos^2\theta/(n^2M+\cos^2\theta+2n\cos\theta M)$$

with $M = 1-n^2\sin^2\theta$.

For the critical angle $< \theta < 90$, it is proportional to :

$$K \times (-M\cos^2\theta)/|\cos\theta+jn(-M)^{1/2}|^2$$

With $\alpha = 0.23k$
and $\beta = 1.45k$,

for quartz substrate, the far field radiation intensity from the above equation is close to the experimental results. This is shown in Fig. 3. This gives us a feeling of both the attenuation and propagation constant of the wave in the wire antenna on a dielectric. The β is the propagation constant of the wave along the wire. It is about 8% less than the propagation constant calculated from the quasi-static approximation [4]. This decrease is consistent with other measured values [5]. The α is the attenuation constant of the current along the wire. With the assumed value, the current will drop by 76% or 12.6 dB for every free space wavelength. This is a relatively large attenuation.

Bibliography

1. N. Engheta, C. H. Papas and C. Elachi, "Interface Extinction and Subsurface Peaking of the Radiation Pattern of a Line Source." **Appl. Phys.** B 26, pp. 231-238, 1981.

2. S. Ramo, J. R. Whinnery and T. Van Duzer, **Fields and Waves in Communication Electronics.** John Wiley and Sons, 1965, Chpt. 12.

3. D. B. Rutledge and M. S. Muha, "Imaging Antenna Arrays." **IEEE Trans Antennas Propagat.**, AP-30, pp. 535-540, 1982.

4. D. B. Rutledge, D. P. Neikirk and D. P. Kasilingam, "Integrated Circuit Antennas." Series on **Infrared and Millimeter Waves**, vol. 10, Academic Press, New York.

5. D. P. Kasilingam and D. B. Rutledge, "Surface-Wave Losses of Coplanar Transmission Lines.", **IEEE/MTT-S Int. Microwave Symposium Digest**, Boston, pp. 113-116, May 1983.

APP3/THE COMPUTER PROGRAM FOR ANTENNA PATTERN MEASUREMENT

```
10 REM TAKE ANALOG DATA AT CHANNEL 3 AND ROTATE
20 REM THE DATA ARE IN THE FILE CALLED "VDATA"
30 REM THE FIRST SIX DATA ARE
40 REM THETA: START ANGLE, RANGE AND STEP
50 REM AND THEN PHE : START ANGLE, RANGE AND STEP
60 REM
70     CLEAR ,14000
80     DEF SEG=7936
90     BLOAD "PCLAB",0
100 REM
110 REM    ANALOG ENTRY POINTS
120 REM
130     ADC.VALUE = 3
140     ADC.ON.TRIGGER=6
150 REM
160 REM    DIGITAL ENTRY POINTS
170 REM
180     ENABLE.FOR.OUTPUT=60
190     OUTPUT.DIGITAL.VALUE=66
200     OUTPUT.DIGITAL.ON.TRIGGER=72
210     SET.TIMEOUT=105
220 REM
230 REM    ANALOG INITIALIZATION
240 REM
250     HIGH.V! = +10!
260     LOW.V!  = -10!
270     RANGE! = HIGH.V! - LOW.V!
280     LSB!=RANGE!/65536!
290 REM
300 REM   DIGITAL INITIALIZAION
310 REM
320     PORT.SELECT%=0
330     D.MASK%=&H1
340     TIMEOUT%=0
350     CALL ENABLE.FOR.OUTPUT (PORT.SELECT%)
360     CALL SET.TIMEOUT (TIMEOUT%)
370     D.STATE%=0
380     CALL OUTPUT.DIGITAL.VALUE
390 REM THE A ARRAY FOR MOTOR ASCII CODES COMMANDS
400     DIM A(10)
410 REM "VDATA" IS THE RESULT DATA FILE.
420     OPEN "VDATA" FOR OUTPUT AS #1
430 REM SET MOTORS VALUES
440 XS=768   :REM X CONTROLLER STATUS ADDRESS
450 YS=769   :REM Y CONTROLLER STATUS ADDRESS
460 DR=770   :REM DATA REGISTER ADDRESS
470 IX=771   :REM INTERRUPT RESET ADDRESS
480 IY=772   :REM INTERRUPT RESET ADDRESS
490 DS=773   :REM DUAL STATUS ADDRESS
500 OUT  YS,190 :REM SET Y TO INITIAL VALUE
510 OUT  XS,190 :REM SET X TO INITIAL VALUE
520 SR=XS   :REM SET DEFAULT CONTROLLER TO X
```

```
530 OUT  SR,0  :REM RESET CONTROLLER
540 OUT  SR,190
550 OUT IX,0:  OUT IY,0 :REM CLEAR X,Y INTERRUPTS
560 CLS
570 INPUT "ENTER 1 FOR 1-D ROTATE AND 2 FOR 2-D";FREEDOM
580 IF FREEDOM=1 THEN GOTO 710
590 PRINT
600 PRINT "FOR 2-D, ALWAYS FIX A THETA AND ROTATE PHE"
610 CTR$="1"
620 PRINT
630 INPUT "ENTER THETA START ROTATION ANGLE"; TSTANG
640 PRINT
650 INPUT "ENTER THETA ROTATING RANGE IN DEGREE"; TRG
660 PRINT
670 INPUT "ENTER THETA ROTATING STEPS IN DEGREE"; TST
680 PRINT
690 INPUT "ENTER + FOR CW,- FOR CCW THETA ROTATION"; TDIR$
700 TST=TST*4 : GOTO 760
710 TSTANG=0 : TRG=0 : TST=4 : TT$="0" : TDIR$="-"
720 PRINT
730 INPUT "ENTER 1 FOR PHE OR 2 FOR THETA ROTATION"; CTR$
740 PRINT
750 PRINT "CALL THE ROTATION AS PHE"
760 CLS : INPUT "ENTER PHE START ROTATION ANGLE"; STANG
770 PRINT :INPUT "ENTER PHE ROTATION RANGE IN DEGREE ";RG
780 PRINT :INPUT "ENTER PHE ROTATION STEPS IN DEGREE"; ST
790 ST=ST*4
800 WRITE #1,TSTANG,TRG,TST,STANG,RG,ST
810 REM generate character equiv. of ST and put it in S$
820     CHAR=ST
830     GOSUB 1850
840     S$=CHA$
850 REM GENERATE CHARACTER EQUIV. OF TST,RESULT IN TT$
860      CHAR=TST
870      GOSUB 1850
880      TT$=CHA$
885 PRINT
890 INPUT "ENTER + FOR CW,- FOR CCW PHE ROTATION" ; DIR$
900 B$=CTR$
910 GOSUB 1720
920 B$="R 180"
930 GOSUB 1480
940 B$="S 35"
950 GOSUB 1480
960 B$="F 9"
970 GOSUB 1480
980 B$="A" : GOSUB 1480
990 FOR TVAR=1 TO 4*TRG/TST+1 STEP 1
1000 B$=CTR$
1010 GOSUB 1720
1020 REM
1030 B$=DIR$ : GOSUB 1480
```

```
1040 REM LOOP TO TAKE A DATA, WAIT AND THEN ROTATE
1050 FOR VAR=1 TO 4*RG/ST STEP 1
1060     GOSUB 1980
1070     WRITE #1,V
1080     SS$=S$
1090     SST=ST
1100      GOSUB 1330
1110 NEXT VAR : GOSUB 1980 : WRITE #1,V
1120 REM rotate motor back to the starting position
1130      REM generate the character equivalent of rg*4
1140      CHAR=RG*4
1150      GOSUB 1850
1160      SS$=CHA$
1170     IF DIR$="-" THEN VDIR$="+" ELSE VDIR$="-"
1180     B$=VDIR$
1190     GOSUB 1480
1200     SST=RG*4
1210     GOSUB 1330
1220   B$="2" : GOSUB 1720
1230   B$=TDIR$ : GOSUB 1480
1240   SS$=TT$
1250   SST=TST
1260   GOSUB 1330
1270 NEXT
1280 REM de-energize the stepper motor
1290      B$="I"
1300      GOSUB 1480
1310 REM PROGRAM ENDS
1320      GOTO 2390
1330 REM stepper motor rotation control
1340     B$="E"
1350     GOSUB 1480
1360     B$="N "+SS$
1370     GOSUB 1480
1380     B$="G"
1390     GOSUB 1480
1400     B$="0"
1410     GOSUB 1480
1420     B$="Q"
1430     GOSUB 1480 : B$="D" : GOSUB 1480
1440     IF SST<20 THEN WSTEP=6*20 ELSE WSTEP=6*ST
1450 REM PROGRAM WAIT TILL MOTOR IS STEADY
1460     FOR DEL=1 TO WSTEP : WASTE =LOG(DEL) : NEXT DEL
1470   RETURN
1480      C=0
1490      J=LEN(B$)
1500      FOR K=1 TO J
1510        C=C+1
1520        S=ASC(MID$(B$,K,1))
1530        IF S=59 THEN S=44
1540       A(C)=S
1550      NEXT K
```

```
1560       IF A(1)=81 GOTO 1590
1570       C=C+1
1580       A(C)=13
1590       OUT SR,190
1600       FOR K=1 TO C
1610         S=INP(SR)
1620         IF S<128 GOTO 1610
1630         OUT DR,A(K)
1640         S=INP(DR)
1650         IF S><A(K) GOTO 1810
1660         OUT SR,62
1670         S=INP(SR)
1680         IF S>=128 GOTO 1670
1690         OUT SR,190
1700       NEXT K
1710 RETURN
1720 REM subroutine of the motor control
1730       OUT XS,0: OUT YS,0: OUT DS,0
1740       ON VAL(B$) GOTO 1750,1760,1770
1750       OUT XS,190: SR=XS: GOTO 1800
1760       OUT YS,190: SR=YS: GOTO 1800
1770       OUT DS,190: SR=DS
1780       IF SR=XS GOTO 1800
1790       IF SR=YS GOTO 1800
1800       RETURN
1810       PRINT "data error: program aborted"
1820       GOTO 2400
1830 REM
1840 REM
1850 REM GENERATE THE CHARACTER EQUIVALENT OF CHAR
1860 REM PUT IT IN CHA$
1870       REM 1st SIGNIFICANT DIGIT
1880       S1=CHAR/100 : S1=FIX(S1)
1890       REM 2nd SIGNIFICANT DIGIT
1900       S2=(CHAR-S1*100)/10 : S2=FIX (S2)
1910       REM 3rd SIGNIFICANT DIGIT
1920       S3=FIX( CHAR-S1*100-S2*10)
1930       CHA$=""
1940       IF CHAR > 99 THEN CHA$=CHR$(S1+48)
1950       IF CHAR >9 THEN CHA$=CHA$+CHR$(S2+48)
1960       CHA$ =CHA$+CHR$(S3+48)
1970 RETURN
1980 REM
1990 REM    ANALOG DATA ACQUISITION
2000 REM
2010      G=4
2020      CHANNEL%=3
2030      GOSUB 2100
2040      REM
2050      REM    DIGITAL OUTPUT
2060      REM
2070      D.STATE%=1
```

```
2080      CALL OUTPUT.DIGITAL.VALUE
2090      RETURN
2100      REM
2110      REM    SET VOLTAGE RANGE
2120      REM
2130      ON G GOTO 2140,2170,2220,2270
2140      GAIN%=500
2150      GOSUB 2310
2160      IF V<.0199 THEN G=4: RETURN
2170      GAIN%=100
2180      GOSUB 2310
2190      IF (.0199<V) AND (V<.0999) THEN G=3: RETURN
2200      IF V>.0999 THEN GOTO 2220
2210      GOTO 2140
2220      GAIN%=10
2230      GOSUB 2310
2240      IF (.0999<V) AND (V<.99) THEN G=2: RETURN
2250      IF V>.99 THEN GOTO 2270
2260      GOTO 2170
2270      GAIN%=1
2280      GOSUB 2310
2290      IF V>.99 THEN G=1: RETURN
2300      GOTO 2220
2310      REM
2320      REM    MEASURE VOLTAGE
2330      REM
2340      SCALED.LSB!=LSB!/GAIN%
2350      CALL ADC.VALUE (CHANNEL%, GAIN%, ANALOG.VALUE%)
2360      VOLTAGE! = (ANALOG.VALUE% * SCALED.LSB!)
2370      V=ABS(VOLTAGE!)
2380 RETURN
2390 CLOSE #1
2400 CLS
2410 END
```